Chapter 1

INTRODUCTION

1-1 Aims of the study

The primary objective of the airborne radiometric mapping in this study was to determine the distribution of the apparent concentration of radioactive elements on the ground surface. The patterns of the distribution, in turn, may be used to assist geological mapping and mineral exploration. Assessment to the usefulness of the airborne data in highlighting prospective areas is of prime importance.

The study includes:

- data processing of the airborne radiometric survey, to produce coloured maps which represent the apparent concentration of radioactive elements potassium (K), equivalent uranium (eU), and equivalent thorium (eTh) on the ground surface;

- comparing the resulting patterns of the distribution of the radioactive elements with the distribution of rock types, taking special notice of areas with known mineralization;

- correlation of the airborne and ground radiometric data in order to examine the quantitative fidelity of the airborne data, and at the same time fully understand the variations in the outcrop-exposure to soil-cover ratio, rock weathering, and other variables;

- a laboratory analysis based on the γ-ray spectra of rocks to determine the relative concentration of radioactive elements in rock samples, and to obtain detailed nature of the primary signal.

An area was chosen because it has been intensively studied geologically and geochemically. The area centres on a body of granite which has produced significant quantities of tin mineralization and lesser tungsten. It was known to have significant abundance of potassium, uranium, and thorium, compared with granitic rocks which have not been responsible for mineralization, and contrasted strongly with surrounding rocks.

1-2 The study area

Geographic location

The study area is situated in north-eastern New South Wales. Figure 1.1 shows the locality of and access to the study area. A small portion to the north-west of the area belongs to the State of Queensland. The study area covers 2 750 square kilometres. In term of the Australian Map Grid system the area is bounded by co-ordinates 340 000 mE; 390 000 mE and 6735 000 mN; 6790 000 mN.

The Bruxner Highway is to the north of the area, connecting Tenterfield in the east and Bonshaw in the west. The New England Highway is to the east of the area. Several sealed and unsealed roads provide easy access when dry to some locations within the area. In wet weather the use of four-wheel-drive vehicles is recommended.

Towns with a mining environment are common in the area. The biggest town is Emmaville, in the south, with a population of approximately 600. Torrington and Stannum are located further into the area. The township of Deepwater is situated on the New England Highway, to the south-east. Homesteads are found sparsely throughout the area. The main activities throughout the region include small-scale mining, minor cropping, and sheep and cattle grazing.

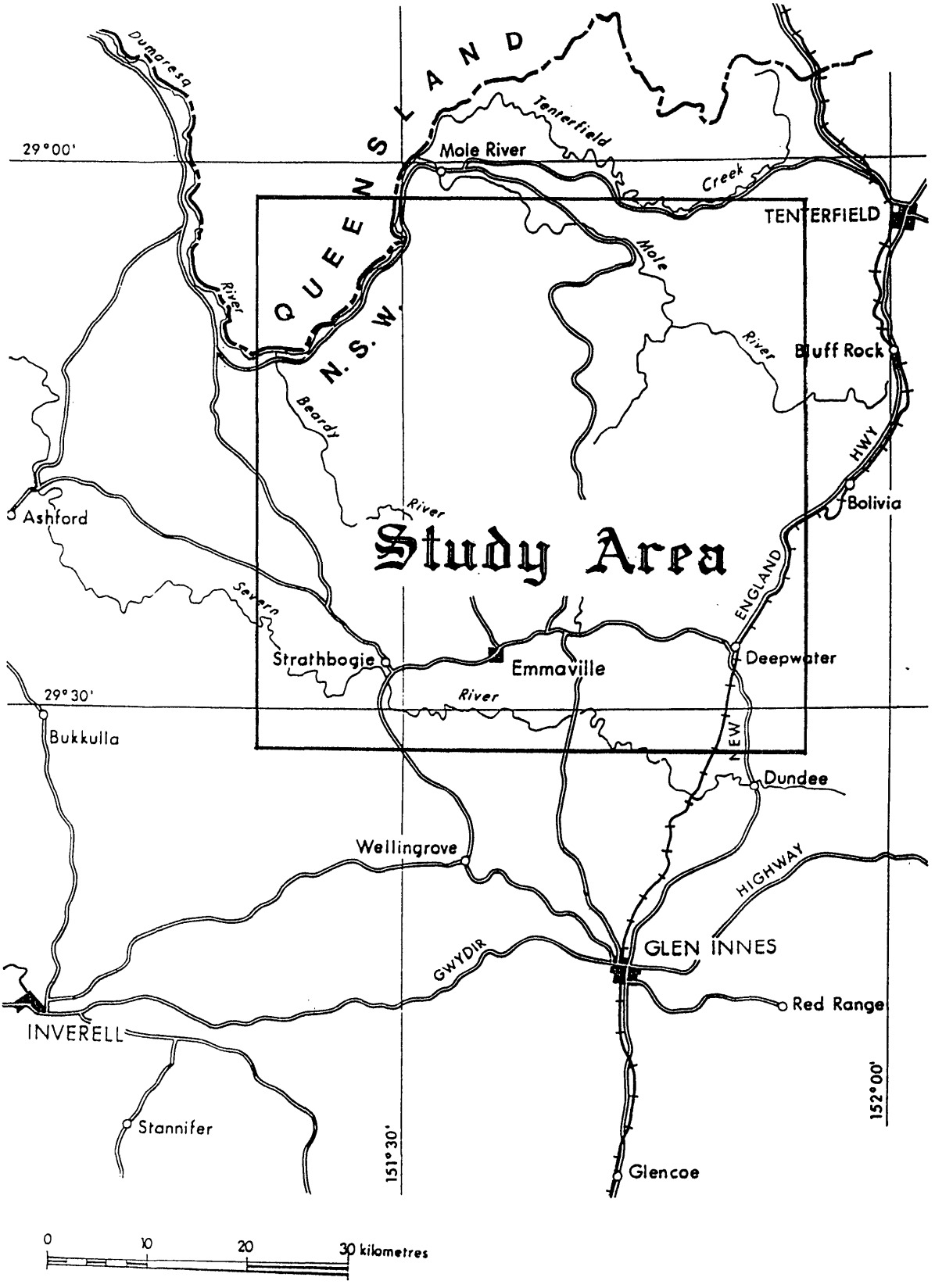

Figure 1.1 Study area: locality and access. (Source: Newmont, 1982).

Physiography

The topography of the study area is generally undulating to hilly. The centre is a dissected tableland, 600 metres higher on average than the surrounding countryside, having a rugged bluff-like character caused by the massive granite. A series of high ranges appear in the east and north-east. The high ranges in the centre are formed mainly by the body of the Mole Granite. The hilly terrain in the north-east and in the eastern part of the area is formed by other granitoid plutons. The sedimentary and volcanic rocks generally form undulating surfaces in the southern and northern part of the area. The topographic elevation of the study area ranges from 400 to 1 300 metres above sea level.

Numerous ephemeral and intermittent streams flow from the high terrain in the centre towards the relatively lower areas with drainage patterns showing 045° - 055° and 315° - 325° directions (Kleeman, 1982). Several perennial rivers exist in the area; these are the Severn, the Beardy, the Dumaresq, the Mole, and the Deepwater rivers.

The climate in the area is generally mild to warm, with a temperature range of 10°C to 25°C in the period of October-April, and of -5°C to 15°C in the period of May-September. The annual average rainfall is approximately 780 millimetres. The driest month is April, with 30 millimetres, and January is the wettest, with 105 millimetres.

Regional geology

The main references used in this brief discussion of the regional geology the study area are the New England geological map with a scale of 1 : 500 000; and the Grafton and Inverell geological sheets with a scale of 1 : 250 000. Several records which describe the geology of the area e.g. Shaw(1964), Lonergan(1971), Brett(1972), Vickery(1972), Godden(1976), Godden(1982), Baillie(1983), Brodie(1983), Stegman(1983), and Cozens(1984) are also cited.

The study area lies within the Woolomin-Texas Block in the central zone of the New England Fold Belt. The block consists of Palaeozoic sediments, which form the basement of the study area. Figure 1.2 shows the geological setting. The regional geology is depicted in Figure 1.3.

Pogson and Hitchin (1973) identified the sedimentary rocks to the north of the Mole Granite as Carboniferous, while the sedimentary facies to the south-west of the granite as a Permo-Carboniferous. The Carboniferous unit is recognized as the Texas Beds. It is composed of lithic-sandstone, mudstone, conglomerate, chert jasper, limestone and andesite. The Permo-Carboniferous unit consists of mudstone, lithic-sandstone, hornfels, pebble conglomerate and ash-flow tuff. Similar sedimentary rocks are found in the Torrington Roof pendant, typically, mudstone, siltstone, conglomerate, and quartzite to quartzose greisen (Pogson and Hitchin, 1973).

The Mid-Permian Bodonga Beds form a north-west-trending ridge on the northern part of the study area. This unit consists mainly of conglomerate, shale, claystone, siltstone, and sandstone (Pogson and Hitchin, 1973).

The Emmaville Volcanics, The Tent Hill Porphyrite, and the Dundee Rhyodacite are the major extrusives which outcrop prominently in the east and south-east part of the study area (Brunker and Chesnut, 1969).

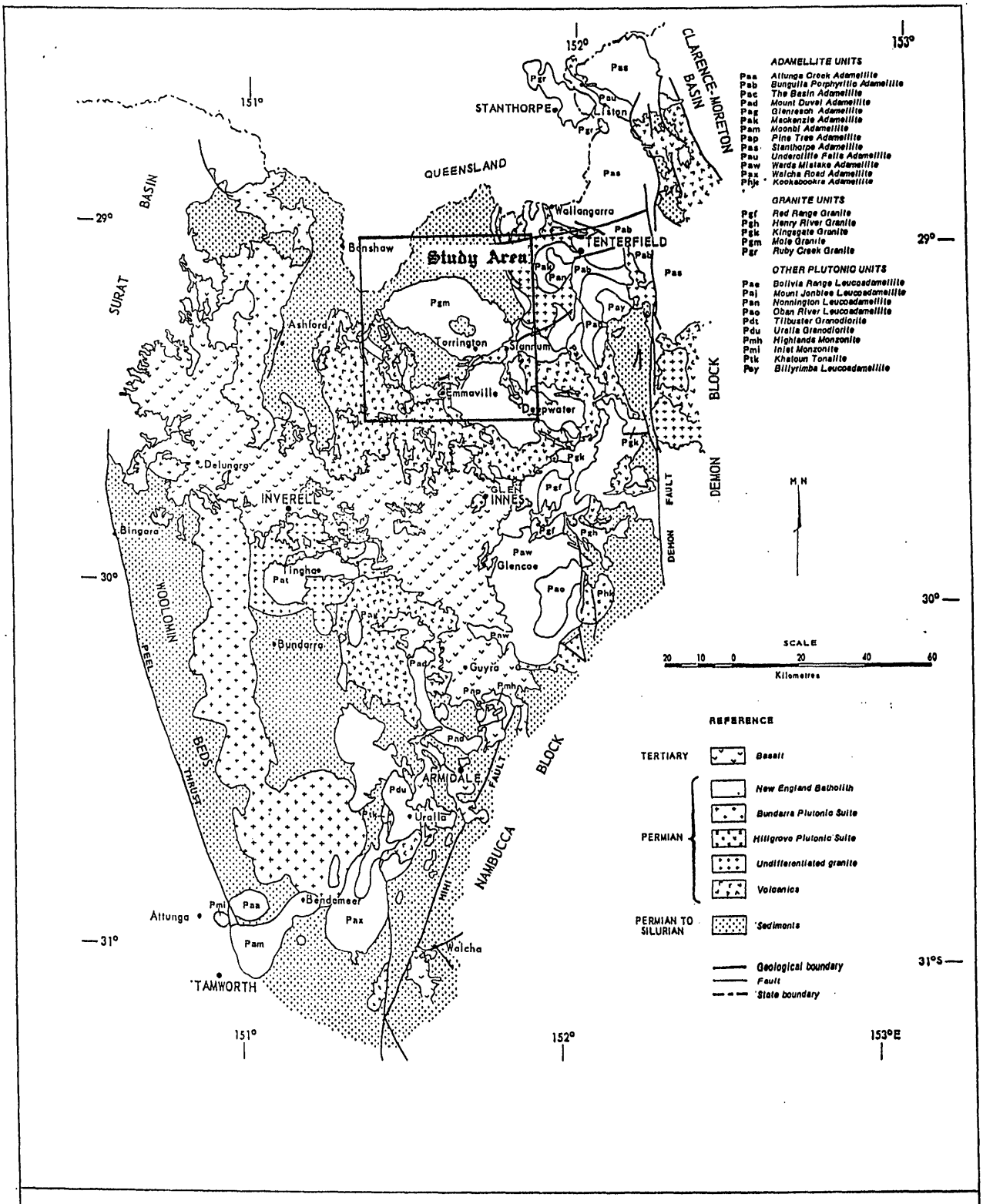

Figure 1.2 Geological setting of the study area.(Source: Weber, 1974).

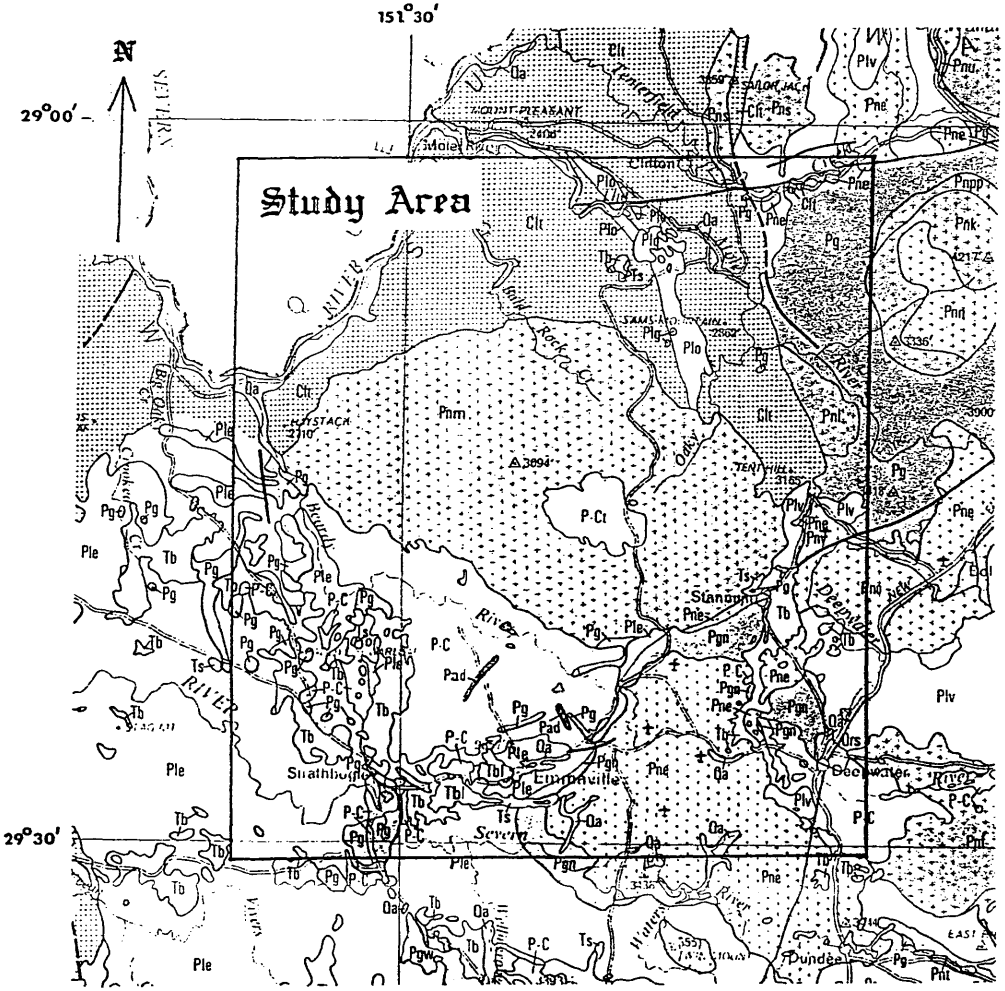

Figure 1.3 Regional geology of the study area

(After New England 1:500 000 Geological Sheet)

The Emmaville Volcanics are located around the township of Emmaville. These units unconformably overlie the Permo-Carboniferous sediments, and also occur as a thin wedge-shaped belt in contact with the Mole Granite (Baillie, 1983). The Emmaville Volcanics consist of four facies (Baillie, 1983); these are rhyolitic ignimbrites, andesitic lavas, breccia and epiclastic sediments.

The Tent Hill Porphyrite conformably overlies the Emmaville Volcanics (Godden, 1976). It outcrops as a long arcuate ridge extending from south of Emmaville northwards to form contact with the Mole Granite (Baillie, 1983). This unit is composed mainly of rhyodacite to dacite facies, porphyritic in texture and dark blue-green in colour (Baillie, 1983).

The Dundee Rhyodacite is the largest extrusive which outcrops in the south-east corner of the study area (Brunker and Chesnut, 1969). Godden (1982) considered that the Dundee Rhyodacite is, mineralogically, similar to the Tent Hill Porphyrite.

The Undifferentiated Granite intrudes the sedimentary basement, particularly to the north-east corner of the study area (Brunker and Chesnut, 1969). Minor outcrops of similar rock appear in the south and west of the area. This unit generally has high mafic content (Brodie, 1983).

The Clive Adamellite outcrops on the eastern part of the study area (Brunker and Chesnut, 1969). It is a coarse-grained equigranular rock, dull-yellow to white in colour (Shaw, 1964).

The Bolivia Range Leuco-adamellite outcrops in an area to the east of the Mole Granite (Brunker and Chesnut, 1969). Shaw (1964) identified the wide-range variation of the texture, grainsize and mineralogy of this unit.

The Gibraltar Ignimbrite unconformably overlies the Bodonga Beds (Brunker and Chesnut, 1969). This unit is a product of pyroclastic flow involving the lateral movement of juvenile volcanic materials as a gravity controlled hot gas or solid dispersion from a vent source (Brodie, 1983).

The Mole Granite outcrops in the centre of the study area. It has 650 square kilometres exposed and rises to 600 metres above the surrounding country (Brett, 1972). It is the most important igneous rock in the study area in that it is, by far, the largest intrusion, and most of the cassiterite-wolframite mineralization is associated with it (Lonergan, 1971). The Mole Granite is a polytextural intrusive, consisting of three principal variants ranging from coarse-grained, porphyritic to microgranitic (Kleeman, 1982).

The Tertiary Basalt encompasses extensive areas, particularly to the south and southwest of the study area (Brunker and Chesnut, 1969). This unit outcrops poorly and commonly forms the bedrock of pasture land (Godden, 1976).

The recent stream alluvials, depending on the country rocks, vary from coarse silica sands to very fine-grained indurated mudstones (Godden, 1976). These units are usually found in low areas of major streams.

1-3 Organization of the thesis

The thesis consists of eight chapters. The present Chapter, the introduction, briefly outlines the objectives of the study, and describes the general features of the study area. Chapter two concerns mainly the theoretical aspects and practical considerations of a γ-radiation survey. Chapter three reviews the previous work in the area, particularly by students and staff members of the Department of Geology and Geophysics of the University of New England, and by other workers in general.

Chapter four introduces the main contribution of the present study by describing the airborne radiometric survey and the data acquired from it. The purpose and the method of the experimental ground radiometric survey are also described in this chapter. The description of the laboratory γ-ray spectrometric analysis is also presented in the same chapter.

Chapter five mainly deals with the data processing. It displays flowcharts of the processing and discusses the computer programs which were used to perform data reduction and filtering. The inverse-filtering method was used to uncover hidden information in the data.

Chapter six presents results of the data processing in the forms of coloured maps of radiometric parameters. These are the maps of the total radiation counts, the apparent ground concentration of potassium (K), the equivalent uranium concentration (eU), and the equivalent thorium concentration (eTh). Maps of the ratios of parameters, namely, eU/K, eU/eTh, and eTh/K, are also presented. Results from the experimental ground radiometric survey provide correlation factors to the airborne radiometric data. In this case, the normalized count rate in the airborne radiometric data may be converted into concentration of every radioactive element. Based on the international standard rock samples GSP-1, AGV-1, G-2, and BCR-1, the laboratory γ-ray spectrometric analysis determines concentration of radioactive elements of rock samples gathered from the field. This analysis was undertaken to verify, with spot analyses, that the overall results from remote sensing were of the correct order.

Chapter seven discusses results from the data processing. The discussion is focused on comparing the distribution patterns of radioactive elements shown by the coloured radiometric maps with the distribution of rock types on the geological map. Special attention is given to account for the coincidence between spots of high radioactive concentration with the already-known prospective areas. In areas where high concentrations are showing, with no marks which show the prospectiveness of the particular areas, further investigations are strongly recommended.

Chapter 2

THEORETICAL ASPECTS AND PRACTICAL CONSIDERATIONS IN A GAMMA - RADIATION SURVEY

2-1 Prelude

In 1906, Sir Ernest Rutherford investigated the radiation from naturally occurring radioactive elements. He also showed that the radiation consisted of three distinct types of emission, namely, α-, β-, and γ-rays.

Each of these rays produces three different effects in varying degree. These are:

- the emission affects photographic emulsion in much the same fashion as light and X-rays;
- the radiation ionizes gas, causing it to become an electrically conducting medium;
- the rays produce scintillation or fluorescence in some minerals and chemical compounds.

These three types of radiation, which are characteristic of natural nuclear disintegrations, have very different penetrating powers. As an illustration of this, α-rays are easily stopped by a sheet of paper, β-rays by a few millimetres of aluminium, whereas γ-rays require several centimetres of lead to stop their travel.

In practical exploration, their equivalent range of penetration in overburden or rocks is essentially zero for both α- and β-rays, and less than a metre for the γ-rays. In fact, this range is a complicated function of the energy and character of the radiation and of the density or effective atomic number of the medium through which the rays travel. The dissipation of energy is a complex process of scattering, collision and absorption involving the atoms of the host material and resulting in ionization along the ray paths. α- and β-rays ionize strongly, in contrast with the weakly ionizing γ-rays.

Apart from the α-, β-, and γ-radiation, there is another type of nuclear transmutation, called K-electron capture, which occurs in several of the natural radioelements (see Table 2-2.1). In this process, an electron from the innermost K-orbit enters the nucleus, which then radiates γ-rays. As a result of this electron-capture process, the atomic number decreases by one, and a different element is created (Telford *et al.*, 1976). Figure 2.1 is an illustration of this process. The equations which represent the transmutation of element X to Y by α- and β-radiation and K-electron capture are given as follows:

$$ {}_pX^{p+n} \longrightarrow {}_{p-2}Y^{p+n-4} + 2He^4 \qquad (\ \alpha \text{ emission}\ ) $$

$$ {}_pX^{p+n} \longrightarrow {}_{p+1}Y^{p+n} + e^- \qquad (\ \beta \text{ emission}\ ) $$

$$ {}_pX^{p+n} \longrightarrow {}_{p-1}Y^{p+n} + e^- \qquad (\ K - \text{electron capture}\ ) $$

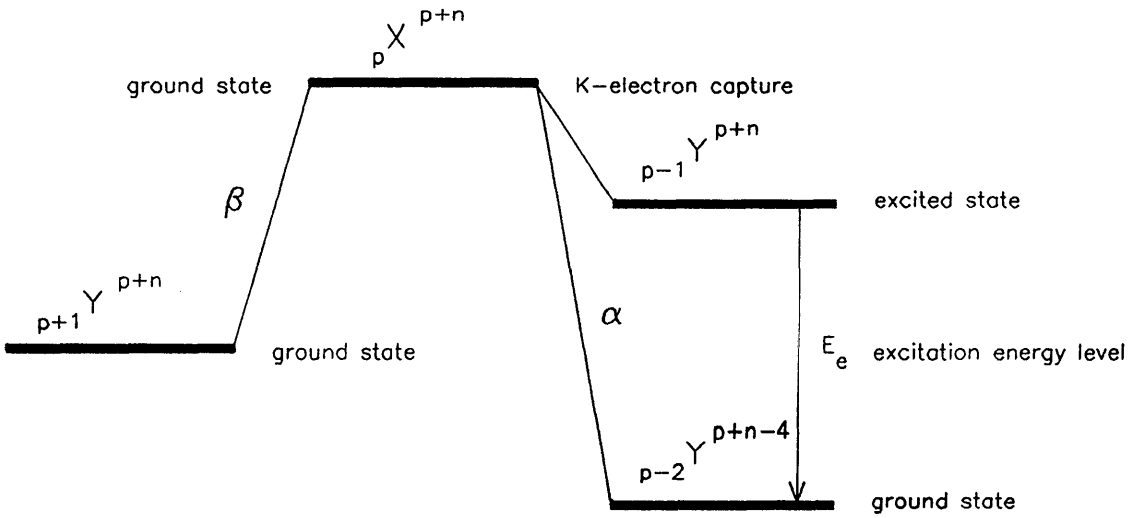

Figure 2.1 Illustrating the transmutation process of element X to Y by α-, and β-radiation and K-electron capture. (Source: Telford *et al.*, 1976).

2-2 Natural radioactive isotopes and radioactivity of rocks and minerals

There are at least twenty naturally occurring elements which are recognized to be radioactive. However, only thorium, uranium, and an isotope of potassium are of importance in exploration. Rubidium, uranium, thorium, potassium, and neodymium are useful radioelements for determining ages of rocks. The other elements are either so rare or so weakly radioactive, or both, that they are considered to be of no significance in the field of applied geophysics.

Table 2-2.1 lists these radioactive elements, together with their characteristic radiation and other pertinent data. Some common radioactive minerals of thorium, uranium, and potassium are listed in Table 2-2.2.

Table 2-2.1

Naturally occurring radioactive isotopes
(Source: Telford *et al.*, 1976)

Element	Isotope	Abundance %	Half-life (years)	Type of radiation	Energy (MeV)
Potassium	$_{19}K^{40}$	0·012	$1·3 \times 10^{9}$	β,K – cap + γ*	1·46
Calcium	$_{20}Ca^{48}$	0·18	$> 2 \times 10^{16}$	β	0·12
Vanadium	$_{23}V^{50}$	0·24	6×10^{15}	β, K – cap + γ*	0·71, 1·59
Rubidium	$_{37}Rb^{87}$	27·8	$4·7 \times 10^{10}$	β	0·27
Indium	$_{49}In^{115}$	95·72	6×10^{14}	β	0·60
Lanthanum	$_{57}La^{138}$	0·089	$1·1 \times 10^{11}$	β, K – cap + γ*	0·54, 0·81, 1·43
Cerium	$_{58}Ce^{142}$	11·1		α	1·5
Neodymium	$_{60}Nd^{144}$	23·8	5×10^{15}	α	1·8
Samarium	$_{62}Sm^{147}$	14·97	10^{11}	α	2·32
Samarium	$_{62}Sm^{148}$	11·2	$1·2 \times 10^{13}$	α	2·14
Samarium	$_{62}Sm^{149}$	13·8	$\sim 4 \times 10^{14}$	α	1·84
Gadolinium	$_{64}Gd^{152}$	0·2	$1·1 \times 10^{14}$	α	2·24
Lutecium	$_{71}Lu^{176}$	2·6	3×10^{10}	β, γ	0·088, 0·20, 0·31
Hafnium	$_{72}Hf^{174}$	0·16	2×10^{15}	α	2·5
Rhenium	$_{75}Re^{187}$	62·9	7×10^{10}	β	$\leq$ 0·008
Platinum	$_{78}Pt^{190}$	0·013	6×10^{11}	α	3·11
Platinum	$_{78}Pt^{192}$	0·78	$\sim 10^{15}$	α	2·6
Lead	$_{82}Pb^{204}$	1·48		α	
Thorium**	$_{90}Th^{232}$	100	$1·39 \times 10^{10}$	α, β, γ	0·03–2·62
Uranium**	$_{92}U^{235}$	0·72	$7·1 \times 10^{8}$	α, β, γ	0·02–0·9
Uranium**	$_{92}U^{238}$	99·3	$4·5 \times 10^{9}$	α, β, γ	0·4–2·5

* K-electron capture followed by γ-ray emission.
** Each of these undergoes a long series of disintegrations yielding lead isotopes 208, 207, 206, respectively. During these disintegrations numerous γ-rays are emitted, in addition to the α- and β-particles.

Table 2-2.2

Radioactive minerals of thorium, uranium, and potassium
(Source: Telford *et al.*, 1976)

Potassium	Mineral	(i) Orthoclase and microline feldspars [$KAlSi_3O_8$] (ii) Muscovite [$H_2KAl(SiO_4)_3$] (iii) Alunite [$K_2Al_6(OH)_{12}SO_4$] (iv) Sylvite, carnallite [KCl, $MgCl_2 . 6H_2O$]
	Occurrence	(i) Main constituents in acid igneous rocks and pegmatites (ii) Same (iii) Alteration in acid volcanics (iv) Saline deposits in sediments
Thorium	Mineral	(i) Monazite [ThO_2 + Rare earth phosphate] (ii) Thorianite [(Th, U)O_2] (iii) Thorite, uranothorite [$ThSiO_4$ + U]
	Occurrence	(i) Granites, pegmatites, gneiss (ii), (iii) Granites, pegmatites, placers
Uranium	Mineral	(i) Uraninite [Oxide of U, Pb, Ra + Th, Rare earths] (ii) Carnotite [$K_2O . 2UO_3 . V_2O_5 . 2H_2O$] (iii) Gummite [Uraninite alteration]
	Occurrence	(i) Granites, pegmatites and with vein deposits of Ag, Pb, Cu, etc. (ii) Sandstones (iii) Associated with uraninite

2-3 Radioactive decay processes

When an element emits α- or β-rays or undergoes K-electron capture process, it transmutes into a new element with a fixed rate of the transmutation, called the decay constant. It is understood that the rate of the change is not affected by physical or chemical processes in the surroundings. For any type of radioactive atom, the following relation holds:

$$\frac{dN}{dt} = -\lambda N \qquad 2-3.1(a)$$

or

$$\frac{dN}{N} = -\lambda\, dt \qquad 2-3.1(b)$$

where dN = the rate of the transmutation;

N = the number of atoms present at time t;

λ = the decay constant.

Performing the integration of both sides of the equation 2-3.1(b) leads to (Telford *et al.*, 1976)

$$\int_{N_0}^{N} \frac{dN}{N} = -\lambda \int_0^t dt \qquad 2-3.2(a)$$

or

$$N = N_0 e^{-\lambda t} \qquad 2-3.2(b)$$

where N_0 = the number of atoms at the beginning of the time interval t.

If $T_{\frac{1}{2}}$ is the period of time required for half of the nuclei to disintegrate, then

$$\text{when} \quad t = T_{\frac{1}{2}}$$

$$\frac{N}{N_0} = \frac{1}{2} = e^{-\lambda T_{\frac{1}{2}}}$$

$$\text{or} \quad \lambda = \frac{\ln 2}{T_{\frac{1}{2}}}$$

$$= \frac{0.693}{T_{\frac{1}{2}}} \qquad 2-3.4$$

In radioactive decay series which initially contain N_0 parent nuclei, after a time interval t, the number N_n of the series is given by the following relation (Adams and Gasparini, 1970)

$$N_n(t) = N_0\left[C_1 e^{-\lambda_1 t} + C_2 e^{-\lambda_2 t} + \cdots + C_n e^{-\lambda_n t}\right] \qquad 2-3.5$$

where

$$C_1 = \frac{\lambda_1\lambda_2\lambda_3\cdots\lambda_{n-1}}{(\lambda_2-\lambda_1)(\lambda_3-\lambda_1)\cdots(\lambda_n-\lambda_1)}$$

$$\cdot =$$

$$\cdot =$$

$$\cdot =$$

$$C_n = \frac{\lambda_1\lambda_2\lambda_3\cdots\lambda_{n-1}}{(\lambda_1-\lambda_n)(\lambda_2-\lambda_n)\cdots(\lambda_{n-1}-\lambda_n)}$$

When the time interval t is very large in comparison with $\lambda_2, \lambda_3, \cdots, \lambda_n$, an equilibrium condition is achieved where

$$N_1\lambda_1 = N_2\lambda_2 = N_3\lambda_3 = \cdots = N_n\lambda_n \qquad 2-3.6$$

This means the rate of transmutation is the same for all members of the series. The ratio of the number of nuclei of each member to that of any other members which are present in the series is inversely proportional to the ratio of respective decay constants.

2-4 The gamma-rays

Gamma-rays are highly penetrating electromagnetic radiation characterized by wavelengths of 10^{-9} metres and shorter or frequencies of 10^{17} hertz or higher. Figure 2.2 depicts the electromagnetic spectrum showing relative bands of wavelengths or frequencies.

Gamma radiation originates from naturally occurring, and artificially produced, radioactive isotopes. In nature these isotopes may be classified as primevals and secondaries. Primeval radioisotopes are those which have sufficiently long half-lives to have survived in detectable amounts since the time of nucleosynthesis.

Secondary radioisotopes are those whose half-lives are too short for them to occur unsupported in detectable amounts at the present time. These radioisotopes are present in nature as a result of decay processes or natural nuclear reactions which involve unstable primeval and stable isotopes.

Three radioactive decay series, from radioisotopes ^{40}K, ^{238}U, and ^{232}Th, are considered to be of great significance in the field of geophysical and geochemical exploration.

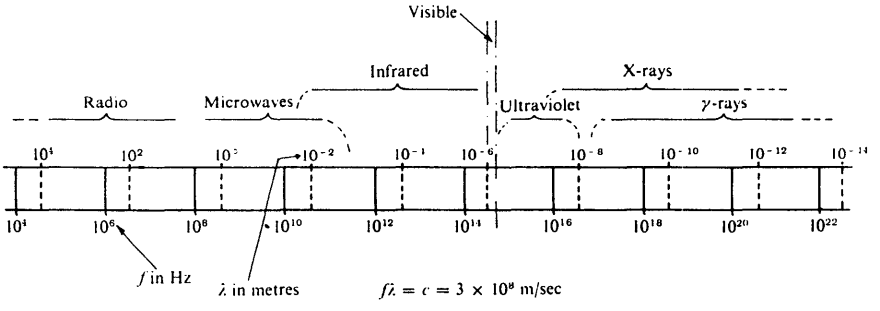

Figure 2.2 Electromagnetic spectrum. (Source: Telford *et al.*,1976).

Radioactive decay scheme of ^{40}K

^{40}K is the only unstable isotope of potassium. Its natural isotopic abundance is 0.0119 . ^{40}K undergoes branched decay either by β-emission to ^{40}Ca (87.6%) or, most commonly, by K-electron capture to ^{40}Ar (12.4%). When ^{40}K transmutes directly to the ground-state of the ^{40}Ca, β-emission occurs, while K-electron capture in most cases produces ^{40}Ar in a 1.46 MeV excited-state, and is then followed by a 1.46 MeV γ radiation.

This radiation is measured for assessing the abundance of potassium when a radiometric investigation is conducted. Figure 2.3 shows the decay scheme of ^{40}K. A typical γ-ray spectrum from potassium is depicted in Figure 2.4 .

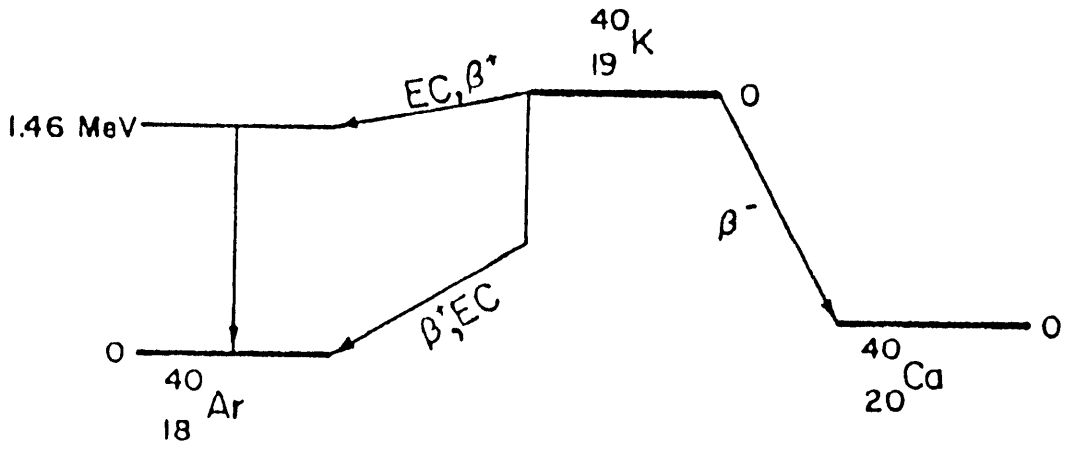

Figure 2.3 Decay scheme of ^{40}K. (Source: Adams and Gasparini, 1970).

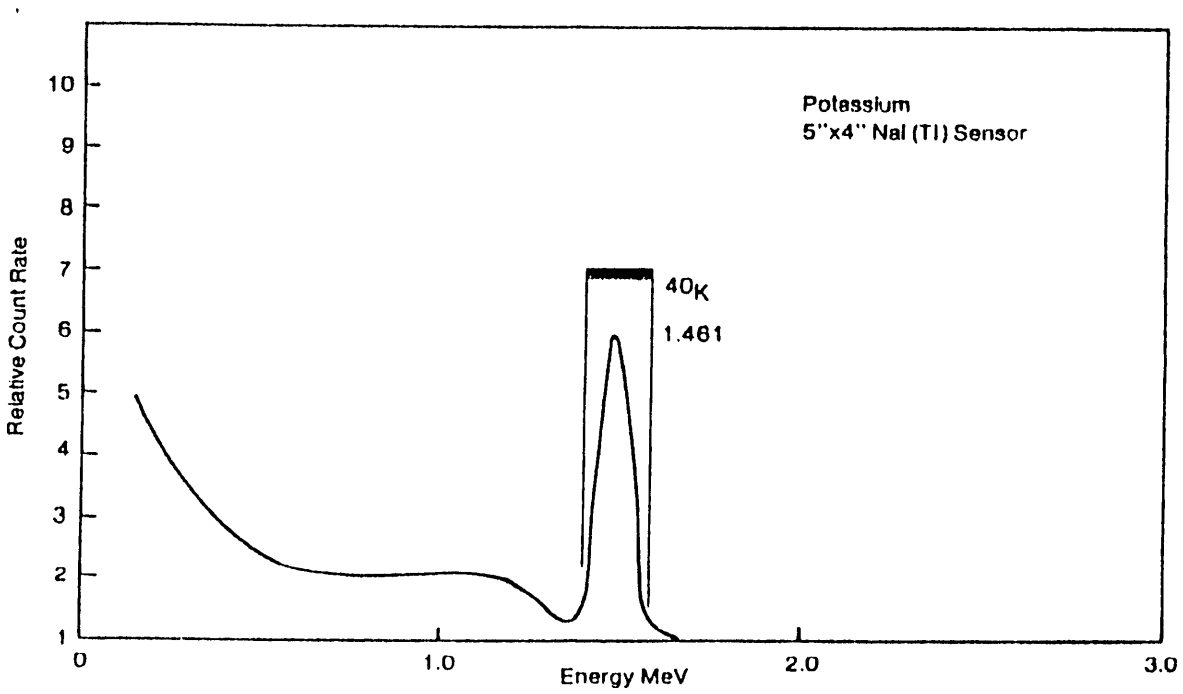

Figure 2.4 Gamma-ray spectrum of potassium. (Source: Scintrex, 1978).

Radioactive decay scheme of ^{238}U

The radioactive decay chain of ^{238}U is shown in Figure 2.5 . The radioisotope ^{238}U is the parent nuclide of the uranium radioactive decay series. This series contains 14 principal daughter nuclides. These include 8 nuclides which are are produced by α-emission and 6 nuclides resulting from β-radiation. Most of these nuclides emit γ-rays of various energies when they undergo decay process. In the decay chain, the members of uranium series may be found together in a state of equilibrium in which a constant abundance ratio is maintained, or disequilibrium may result from disturbance of one or more of the intermediate daughter nuclides by chemical processes in a particular environment.

Figure 2.6 shows a typical γ-ray spectrum obtained from pitchblende, a uranium-rich compound. The spectrum resulting from the equilibrium uranium decay series is rather complex due to the many different γ-ray energies. Quantitative measurement may be made by selecting a suitable characteristic spectral peak in the series. Uranium itself does not produce a suitable characteristic γ-ray. The spectral peak at energy 1.76 MeV which is due to ^{214}Bi is used for assessing the abundance of equivalent uranium in rocks, in remote sensing applications. A number of other peaks in the spectrum can be used in controlled laboratory applications, but these are not used for geophysical exploration work, because they are of lower energy, and require high resolution spectrometers.

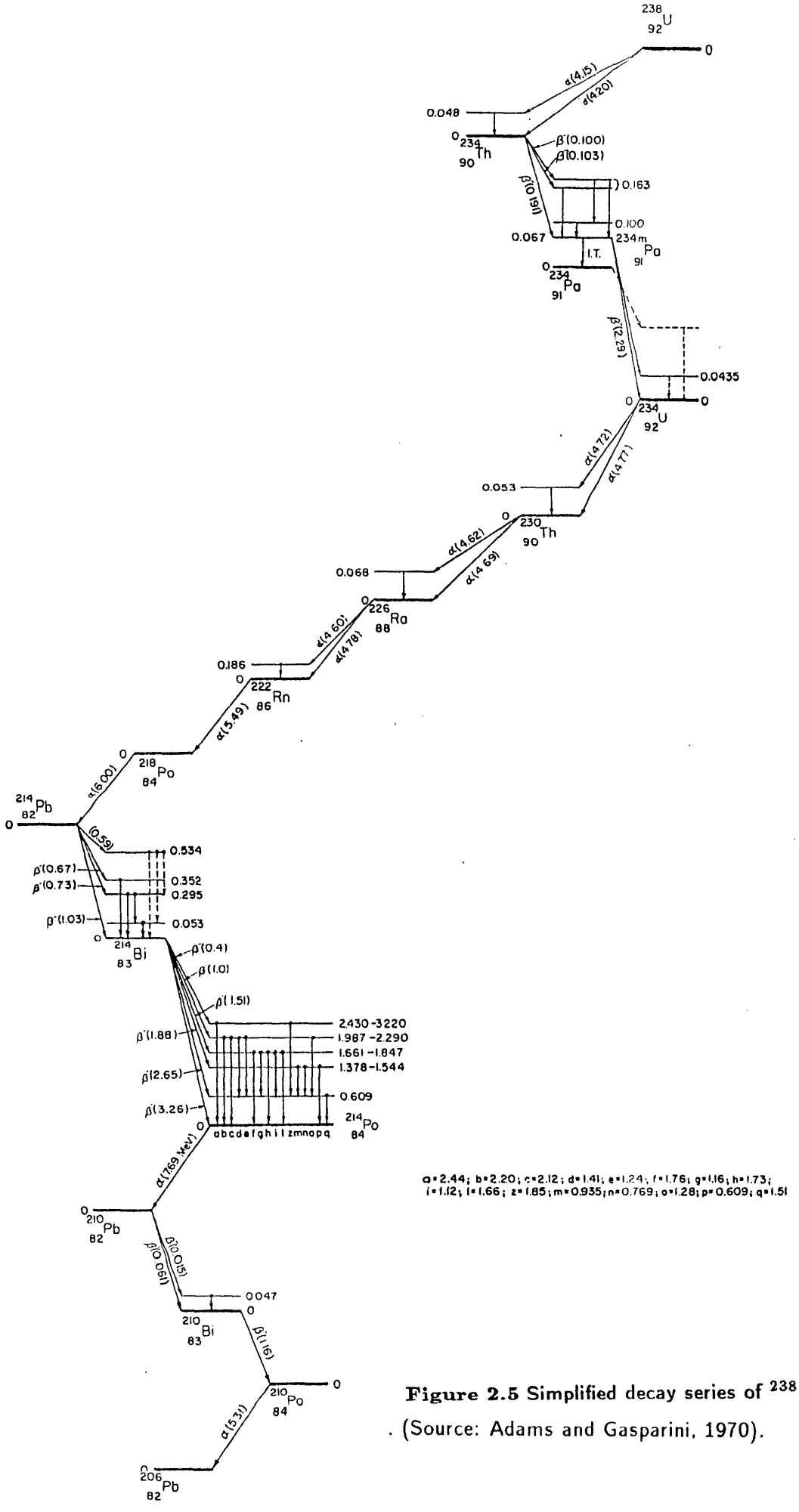

Figure 2.5 Simplified decay series of ^{238}U. . (Source: Adams and Gasparini, 1970).

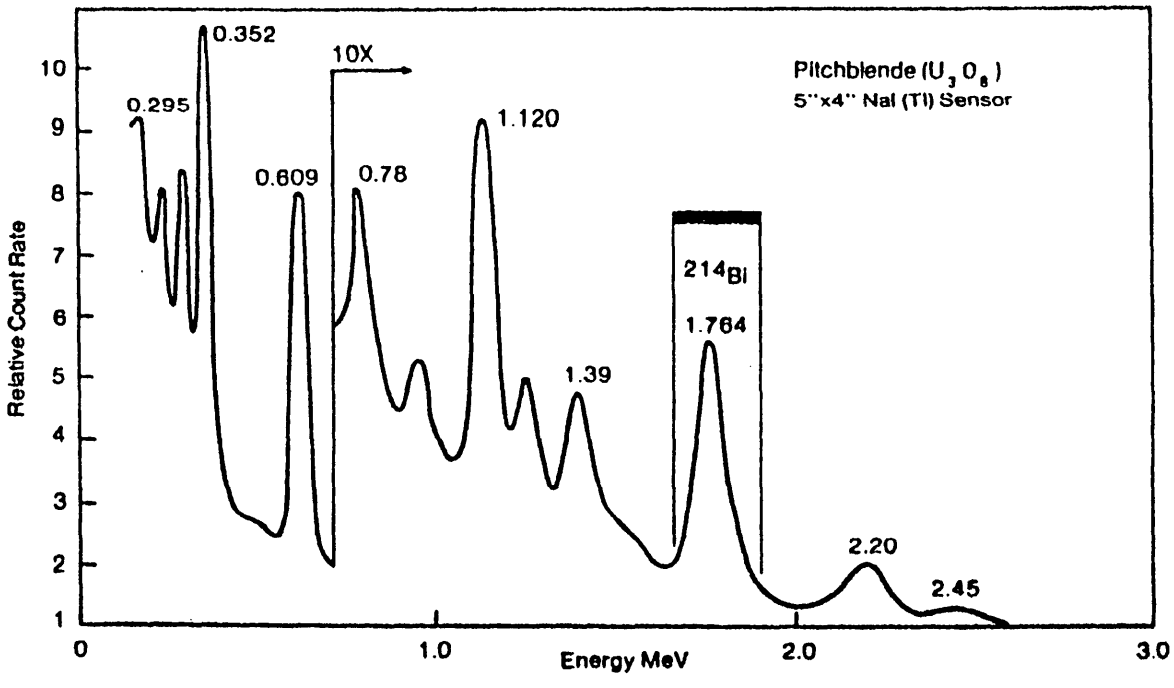

Figure 2.6 Gamma-ray spectrum obtained from pitchblende. (Source: Scintrex, 1978).

Radioactive decay scheme of ^{232}Th

The radioisotope ^{232}Th is the parent nuclide of the thorium radioactive decay series. This series has 11 principal daughter nuclides. Figure 2.7 shows the thorium decay series. A typical γ-ray spectrum observed from a thorium sample is depicted in Figure 2-8 .

The complex γ-ray spectrum shown in Figure 2.8 results from the many different γ-ray energies emitted by the daughter nuclides in the series when they decay.

For the purpose of exploration, the most suitable characteristic γ-ray peak in the thorium series occurs at 2.61 MeV which is due to the radioisotope ^{208}Tl. Thus, this radiation is measured for assessing the equivalent thorium concentration in rocks.

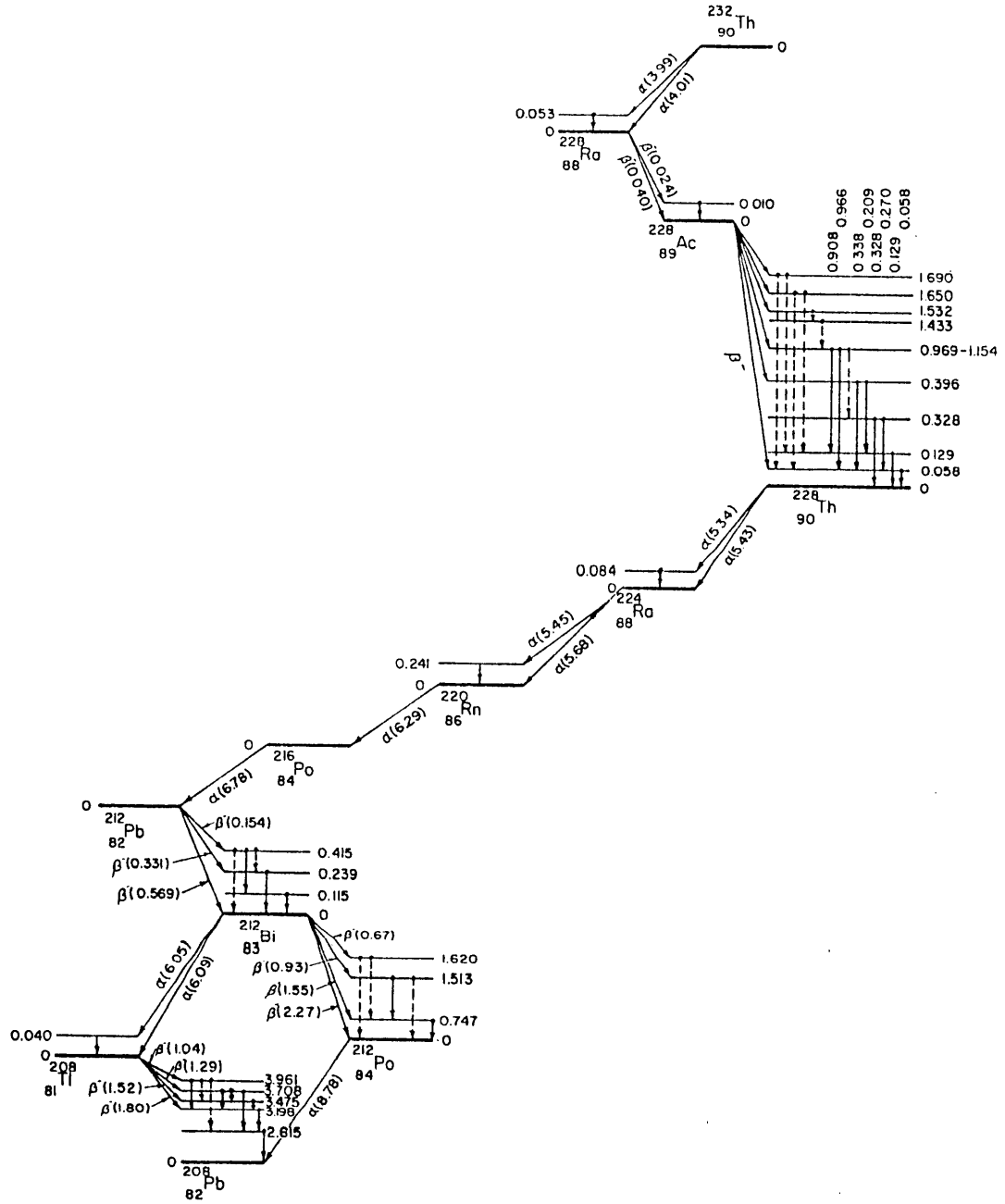

Figure 2.7 Simplified decay scheme of ^{232}Th. (Source: Adams and Gasparini, 1970).

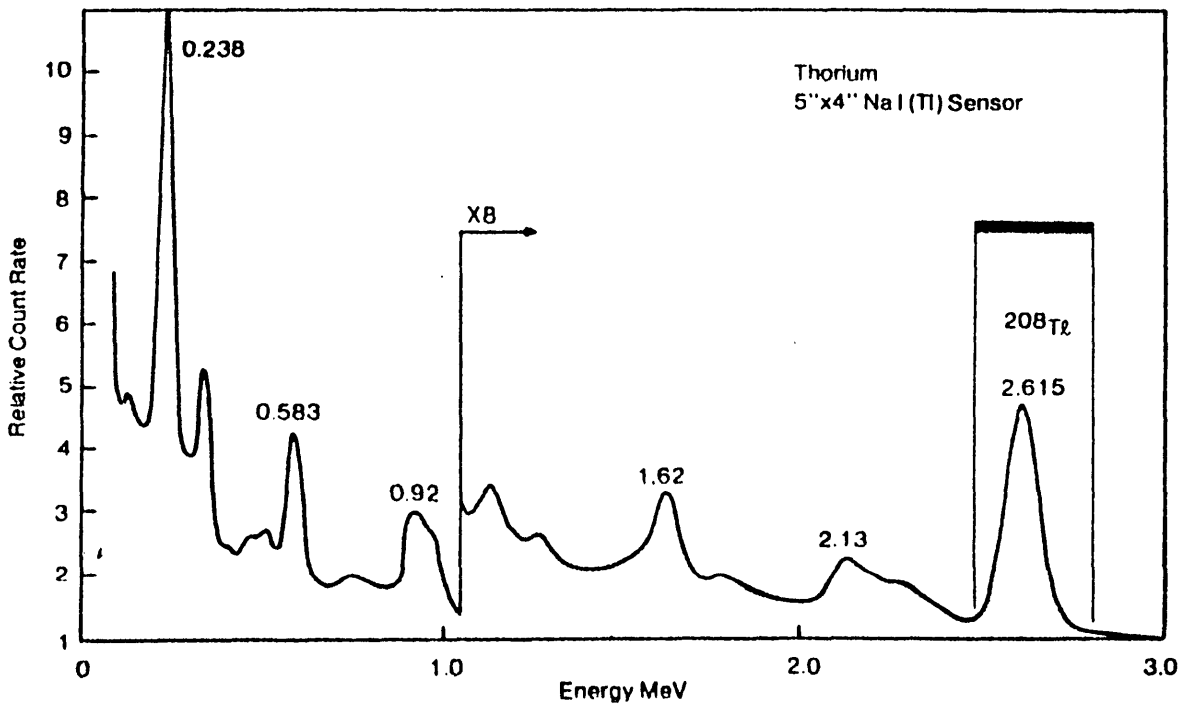

Figure 2.8 Gamma-ray spectrum of thorium sample. (Source: Scintrex, 1978).

Background radiation of gamma-rays

Apart from the three main sources of γ-rays which are utilized in geophysical or geochemical exploration, there is always a certain low level of radiation in nature, even in the absence of geological deposits K, U, and Th. This level is referred to as radiation background which is mainly caused by

- *cosmic rays;*
- *nuclear fallout;*
- *airborne radon; and*
- *trace radioactivity.*

Cosmic rays

Cosmic rays are energetic quanta which originate from extra-terrestrial sources. These rays produce a low-flux, high-energy radiation level in the atmosphere. At elevations of 1000 metres and higher above sea level, cosmic radiation becomes dominant.

Nuclear fallout

In nuclear explosions, radioactive nuclides are spread over the earth's surface and atmosphere in varying amounts. These explosions produce γ-ray radiation at less than 1 MeV energies. Thus, this radiation does not produce interference in the quantitative work in γ-ray exploration which is based on higher characteristic energies.

Airborne radon (atmospheric γ-rays)

The atmosphere contains varying amounts of natural radioactive nuclides. The most important nuclide is ^{222}Rn and its daughter product ^{214}Bi. These amounts are subject to strong fluctuations at times and can cause significant anomalies in spectrometric data. An assembly of upward-looking crystal detectors is often employed for the purpose of monitoring these fluctuations during an airborne γ-ray survey.

Trace radioactivity

Minor amounts of the naturally occurring radioactive elements appear in most rocks and soils. These contribute a low-level background radiation in nature.

2-5 Interaction of gamma-rays with detectors

Gamma-rays interact with a detector in three primary processes. These include

- *the photoelectric process;*
- *the Compton scatter process; and*
- *the electron-positron pair production process.*

In these three processes, γ-rays transfer all or part of their energy to the detector from which output signals may be observed. The output signal determines the characteristic of the photon energy of the incident γ-rays. The signal arising from the total energy absorption is the fundamental basis for γ-ray spectrometric analysis. In this analysis, a photo-peak energy of particular γ-ray photons can be examined when observation of the photon energy versus signal count rates is made. Figure 2.9 shows a typical γ-ray spectrum of potassium bromide obtained with a thallium-drifted sodium-iodide crystal detector.

Total absorption of monoenergetic γ-ray by a detector may result in a single-line spectrum at that photon energy. This photo-peak energy is essentially Gaussian in shape rather than a single line. This Gaussian-shaped energy spectrum has finite width due to statistical variation in the detection process and non-proportional response of the detector system. The narrower the peak, the better the resolution and usually the more useful the detector is for the γ-ray spectrometric analysis.

Figure 2.10 shows partial absorption curves for three interaction processes in three types of detector materials, anthracene, germanium, and sodium iodide.

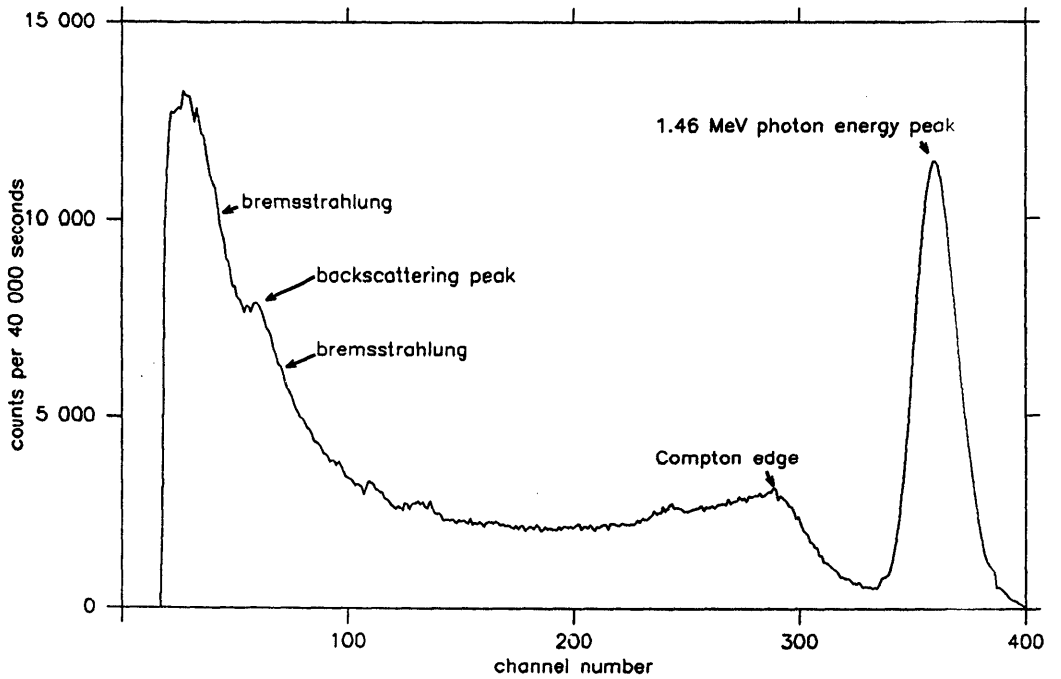

Figure 2.9 Gamma-ray spectrum observed from potassium bromide.

The photoelectric process

Each γ-ray photon has a kinetic energy E_γ which depends only on its frequency ν or wavelength λ

$$E_\gamma = h\nu = \frac{hc}{\lambda} \qquad 2-5.1$$

where h = Planck constant;

c = speed of electromagnetic wave in vacuum ($3.0 \times 10^8 \text{ms}^{-1}$).

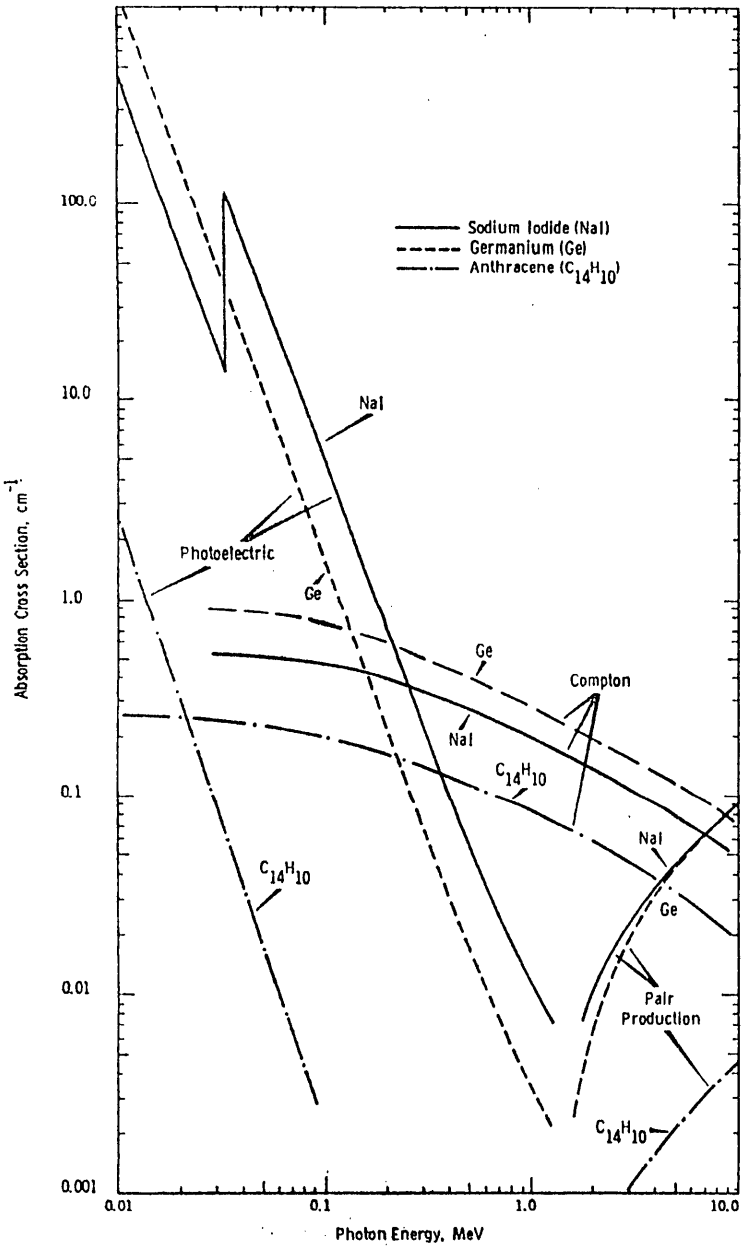

Figure 2.10 Partial absorption coefficient curves for three interaction processes in three types of detector materials. (Source: Adams and Gasparini, 1970).

Upon collision with an electron, the incident photon transfers all of its kinetic energy to an electron. If this energy exceeds the binding energy of the electron E_b, the electron is expelled from the atom with a kinetic energy E_x, where

$$E_x = E_\gamma - E_b \qquad 2-5.2$$

The converse effect holds, that is, when an electron loses its kinetic energy, it creates a photon. If this photon has an energy which corresponds to an electromagnetic frequency in the visible light, a flash of light will be observed (assuming the photon density is great enough for the eye to detect). In practice there are usually not sufficient photons for visual detection and an amplifier with associated electronics can be built which essentially counts the number of photons. This is the principle of the photomultiplier and NaI(Tl) crystal detector which is used in exploration work.

Compton scatter process

In the Compton scatter process the photon transfers only part of its energy to an electron. This process takes place when a γ-ray interacts with a free or loosely bound electron in the outermost orbit of an atom. As a consequence of the partial energy loss, the scattered photon has a lower frequency as shown in Figure 2.11 . The energy of a photon scattered at an angle θ can be approximately evaluated with the following relation

$$(h\nu)_\theta = \frac{(h\nu)_0}{1 + \frac{(h\nu)_0}{mc^2}(1 - cos\theta)} \qquad 2-5.3$$

where $(h\nu)_0$ = the initial energy of the photon;

mc^2 = the rest energy of the electron (0.511MeV).

Electron-positron pair production process

In this process an electron-positron pair is created in the field of a nucleus or an electron which must be present to conserve momentum and energy. This process requires energy equivalent to two electrons rest energy (1.02 MeV). therefore, only a photon with at least that energy can initiate the process.

After the pair has been formed, the positron is slowed down by interaction with electrons and its energy gradually decreases to the rest energy. Then annihilation process occurs in which a positron combines with an electron. The rest energy of the two mutually annihilating particles is transformed into radiant energy, two γ- rays of 0.511 MeV which are emitted in almost opposite directions (Adams and Gasparini, 1970).

The electron-positron pair production process is less significant compared with the photoelectric and Compton scatter processes. Figure 2.12 shows regions of domain of these three interaction processes indicating a domain for common rocks.

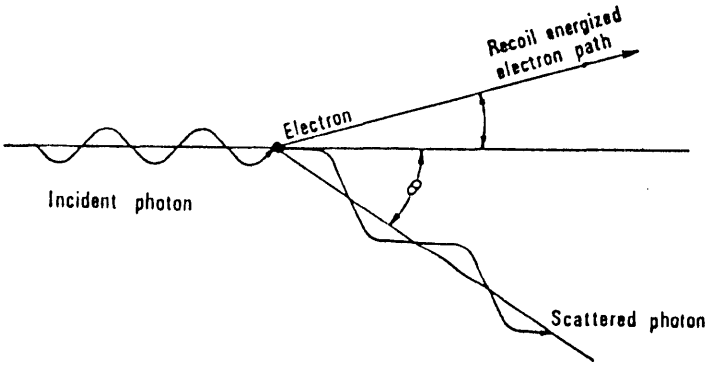

Figure 2.11 Diagrammatic representation of the Compton scattering process. (Source: Adams and Gasparini, 1970).

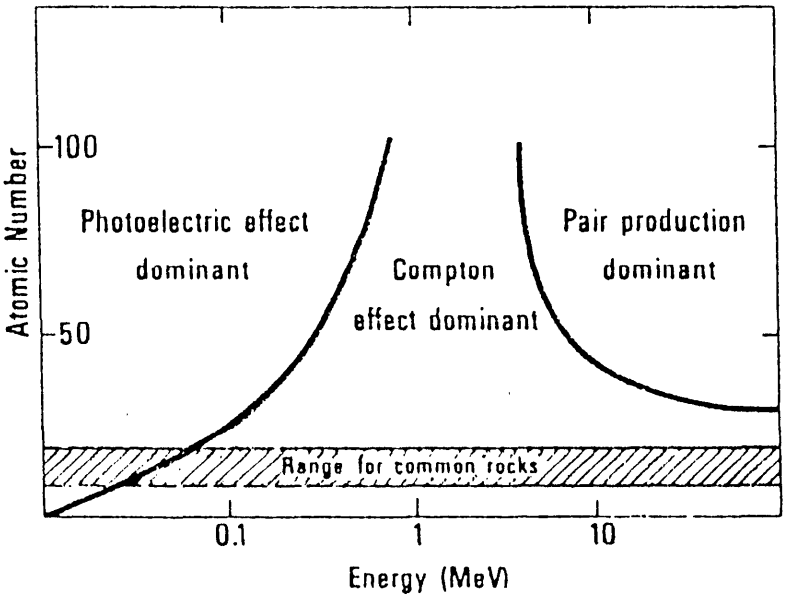

Figure 2.12 Illustrating γ-ray reactions which depend on atomic number and photon energy. (Source: Beck, 1980).

2-6 Gamma-ray detecting system

The most frequently used instrumentation for measuring γ- radiation in the field of geophysical and geochemical exploration is a scintillation-detector system. This system is usually comprised of a thallium-drifted sodium-iodide, (NaI(Tl)), crystal(s) detector assembly which is housed together with a photomultiplier tube, the preamplifier, and the power-supply system, in a thermally insulated package. The sensor assembly is coupled to a spectrometer in which signal processing and the measurement take place.

Figure 2.13 is a diagram of a typical γ-ray detector system capable of measuring the full spectrum of γ-rays as well as the discrete four energy channels registering the total counts, potassium, uranium, and the thorium radiation intensities.

In a scintillation-detecting system, the interaction of γ-rays and the crystal detector causes the crystal to produce pulses of visible light. The total light-flux is proportional to the amount of energy deposited by the γ-rays in the crystal. The photomultiplier, which is optically coupled to the crystal detector, converts the pulses of light into small electronic pulses which are also amplified. The high-voltage power supply provides bias to the photomultiplier to permit amplification of the light pulses. The preamplifier sets the height of the amplified pulses proportional to the energy of individual γ- rays which have been detected.

Gamma-ray spectroscopy is performed by pulse-height analyzers. The four single-channel analyzers process the individual energy-windows of potassium, uranium, and thorium as well as the total radiation counts. A full spectrum of γ-ray energy is processed by the multichannel pulse-height analyzer.

Digital as well as analogue outputs of the instrument permit on-the-spot data evaluation and subsequent data processing on a computer.

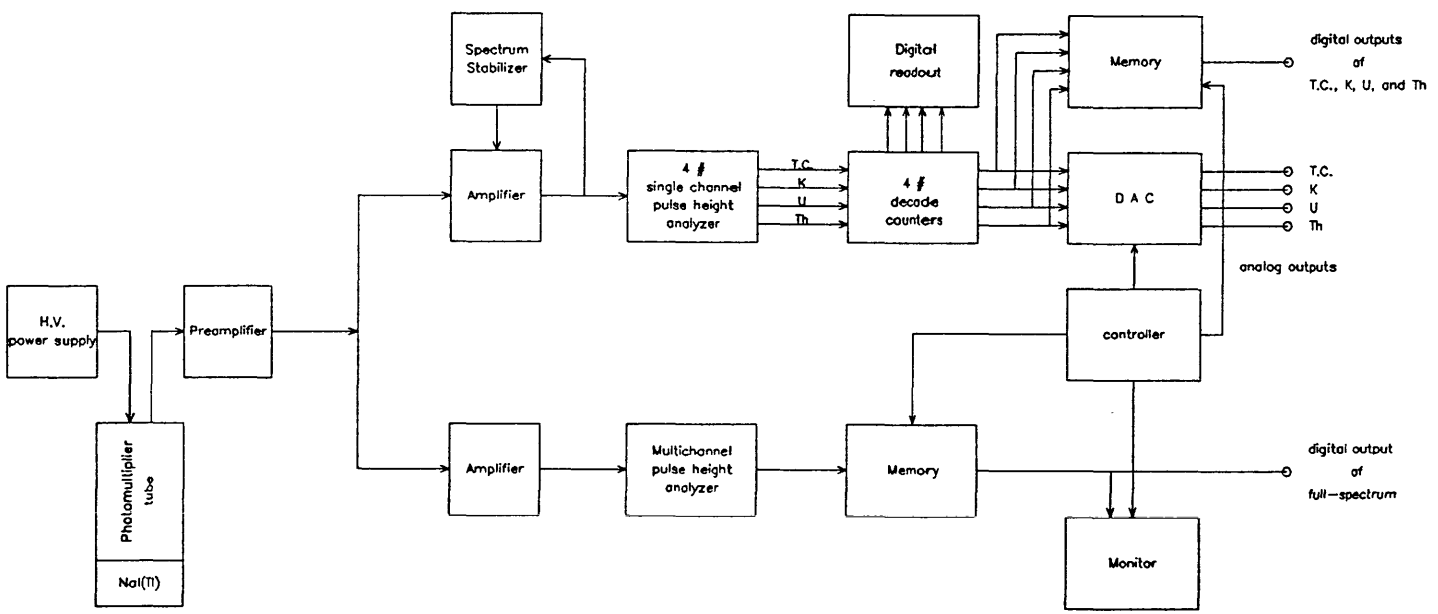

Figure 2.13 A diagram of a γ-ray detecting system capable of measuring a full spectrum and discrete four channels registering TC, K, U, and Th.

2-7 Gamma-radiation surveys

The general objective of γ-ray spectrometric investigations is to locate anomalous radiation fields and to determine the nature and concentration of radioisotopes which give rise to the anomalies. The technique of measuring the radiation is simply to move the spectrometer across or through the area of interest. This may be performed in a systematic manner on a grid pattern for both prospecting and mapping purposes. Prospecting may also utilize random measurements along irregular traverses.

In order to maintain the accuracy of the measurement, calibration of the energy windows of the spectrometer must be performed before a survey is started, and examined periodically thereafter. Consistent reading on the calibrations assure the operator that the instrument is set correctly and operating properly.

The background count rate for each energy window should be measured and recorded before the beginning of the survey each day, and if necessary, a periodical check may also be made. Background measurements may be conducted over a body of water where possible, or on a selected low-radioactivity area such as an area with deep weathering or extensive soil cover.

The total count channel measures all γ-rays of energy 0.40 - 3.0 MeV and is, therefore, the most sensitive indication of any change in the total γ-radiation flux. It is not sensitive to changes in the nature of the γ-ray spectrum. Because of its sensitivity, this channel is the most practical to utilize for reconnaissance work. The potassium (K), uranium (U), and thorium (Th) are used to indicate the nature and concentration of the radioisotopes which produce the radiation field.

In mobile surveying, the speed of traversal of the sensor past an anomaly or area of interest will have an effect on the quality of the measured signal. The speed of traversal and the height of the detector should be chosen so that the desired definition of a selected minimum anomaly is achieved.

The geometry of the γ-ray source and the detector system which is used in measurements affects the signal strength for a particular instrument configuration. In a ground survey, for example, the effective radiating area is large compared with the detector size and source-detector distance. In this case, the source detector solid-angle is approximately 2π. In an airborne survey, the geometry of source and detector varies considerably due to the changes in altitude and geometry of the source. Variation can occur from a point-source (a high-grade boulder) to a 2π-source (a large plane of surface).

Ground surveys

A ground radiometric survey is usually conducted to cover a small area or selected survey lines as the follow-up work of airborne mapping. Vehicle-mounted or hand-carried surveys are conducted close to, or in contact with, the exposed surface of the source of radiation. A larger volume of crystal detector is usually required for vehicle-borne surveys. Due to increased volume, the measured count rate is dependent upon the speed of traversal of the vehicle. A data-acquisition system is usually employed in this type of survey.

Airborne surveys

This type of survey is capable of covering a vast area inaccessible by ground work. The equipment used in an airborne radiometric survey is usually far more sophisticated and expensive than the equipment used in a ground survey. An airborne survey generally employs both differential mode registering the four channels energy measurement which include total radiation counts (TC), potassium counts (K), uranium counts (U), and thorium (Th), as well as recording the full spectrum of γ-ray radiation from the source. The measurements are usually recorded on a dedicated data-acquisition system permitting further processing on a mainframe or minicomputer.

Because of the limited range of γ-ray radiation, this method is generally used as a regional geological mapping tool to determine the distribution of major rock units. Flight altitude is limited to 100 to 500 metres above the ground level since at greater elevations, secondary γ-rays from cosmic ray interactions in the atmosphere begin to dominate.

The flight altitude governs the anomaly resolution by the following expression (after Kileen *et al.*, 1970)

$$\lambda_c = \frac{h_c}{2} \qquad 2 - 7.1$$

where h_c is the maximum altitude permissible for the detection of anomalies of minimum wavelength λ_c. From digital sampling theory it is understood that the sampling rate of a space-varying function affects the folding point in the wavelength domain, in which shorter spectral wavelength components are folded back (aliased) and contribute power to the longer wavelength components. This wavelength, which is called Nyquist wavelength, is represented as

$$\lambda_N = 2V\Delta t \qquad 2 - 7.2$$

where λ_N = the Nyquist wavelength;

V = aircraft speed (ms^{-1});

Δt = sampling interval in time (seconds).

To minimize the aliasing effect, the Nyquist wavelength λ_N which is governed by the sample rate should be less than that controlled by flight altitude λ_c. However, for best practical application in radiometric counting statistics, the sampling rate should be minimized. For the sake of compromise, equating λ_c and λ_N yields an optimum sampling time as a function of altitude, for the desired anomaly resolution, and velocity of

$$\Delta t_{op} = \frac{h_c}{4V} \qquad 2 - 7.3$$

where Δt_{op} = optimal sampling interval in time (seconds).

To compensate for the sampling-interval minimization, aircraft speed, and the permissible flight altitude, a large volume NaI(Tl) crystal detector assembly is generally used to maintain the optimization of the detection. Figure 2.14 shows the optimized sampling interval versus flight altitude for several flight speeds. Figure 2.15 depicts the predicted count rate per litre of NaI(Tl) crystal detector as a function of altitude above ground level for specific radioelement concentrations.

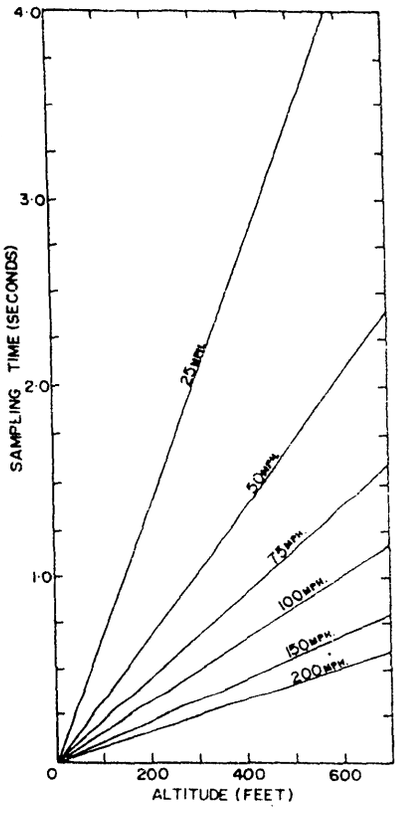

Figure 2.14 Sampling interval as a function of flight altitude for several flight speeds. (Source: Killeen *et al.*, 1970).

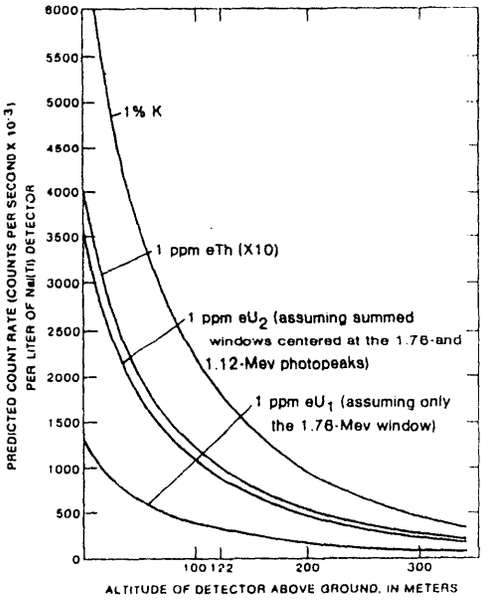

Figure 2.15 Predicted count rate per litre of NaI(Tl) detector as a function of altitude above ground level for specific radioelement concentrations. (Source: Pitkin and Duval, 1980).

Chapter 3

PREVIOUS STUDIES

3-1 Status of the study area since 1960

Figure 3.1 shows the areas covered by previous work on geology, mineralization, and geophysics in the study area. Within the last two decades, the study area has been intensively explored, particularly by students and staff members of the Department of Geology and Geophysics of the University of New England, and by other workers in general.

In 1963, Clark investigated the geology and mineralization in the Emmaville area. Shaw (1964) studied the petrology of a portion of the New England Batholith in the Tenterfield region. Lonergan (1971) examined ore deposits in the southern half of the Mole Tableland. In 1972, Brett investigated some geochemical and petrological aspects of tin mineralization within the Mole Granite, and Vickery studied the geology of the Mole River valley. Godden (1976) explored the volcano-plutonic association in north-eastern New South Wales.

Flinter et al. (1972), Juniper and Kleeman (1979), and Flinter (1981, 1982) described the Mole Granite as , chemically a "tin-mineralizing" type. In 1982, Kleeman recognized the "A - type" affinities of the Mole Granite. Weber (1974) published aspects of mineral deposits associated with plutonic rocks and the intruded sediments on the Woolomin-Texas Block. Figure 3.2 shows mineral deposits found in the Mole Granite and surrounds.

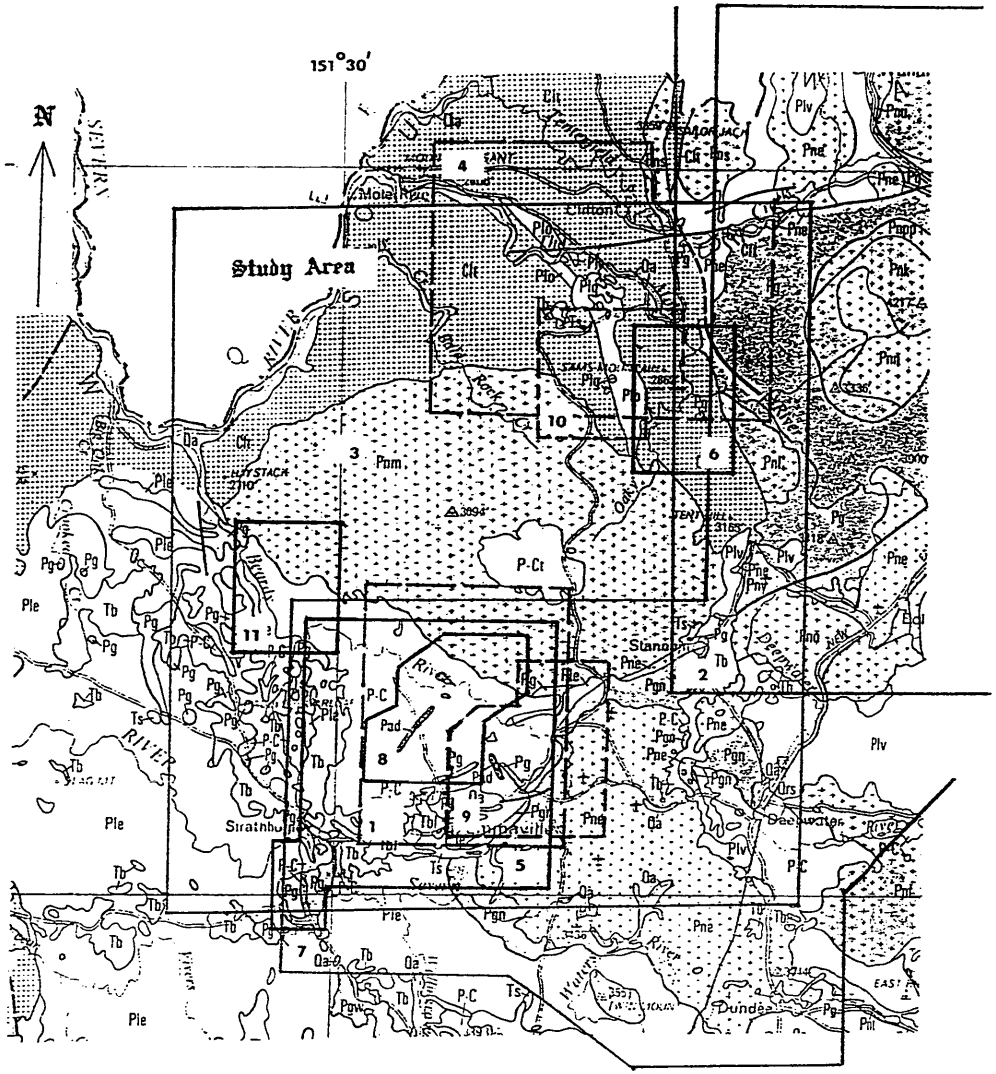

Figure 3.1 Previous work on geology, mineralization, and geophysics in the study area and surrounds.

1. Clark, 1963
2. Shaw, 1964
3. Brett, 1972
4. Vickery, 1972
5. Godden, 1976
6. Clark, 1981
7. Godden, 1982
8. Stegmann, 1983
9. Baillie, 1983
10. Brodie, 1983
11. Cozens, 1984
12. B.M.R., 1970 (Regional Gravity Survey)
13. Geol. Survey NSW (Regional Magnetic Survey)

(After New England 1:500 000 Geological Sheet)

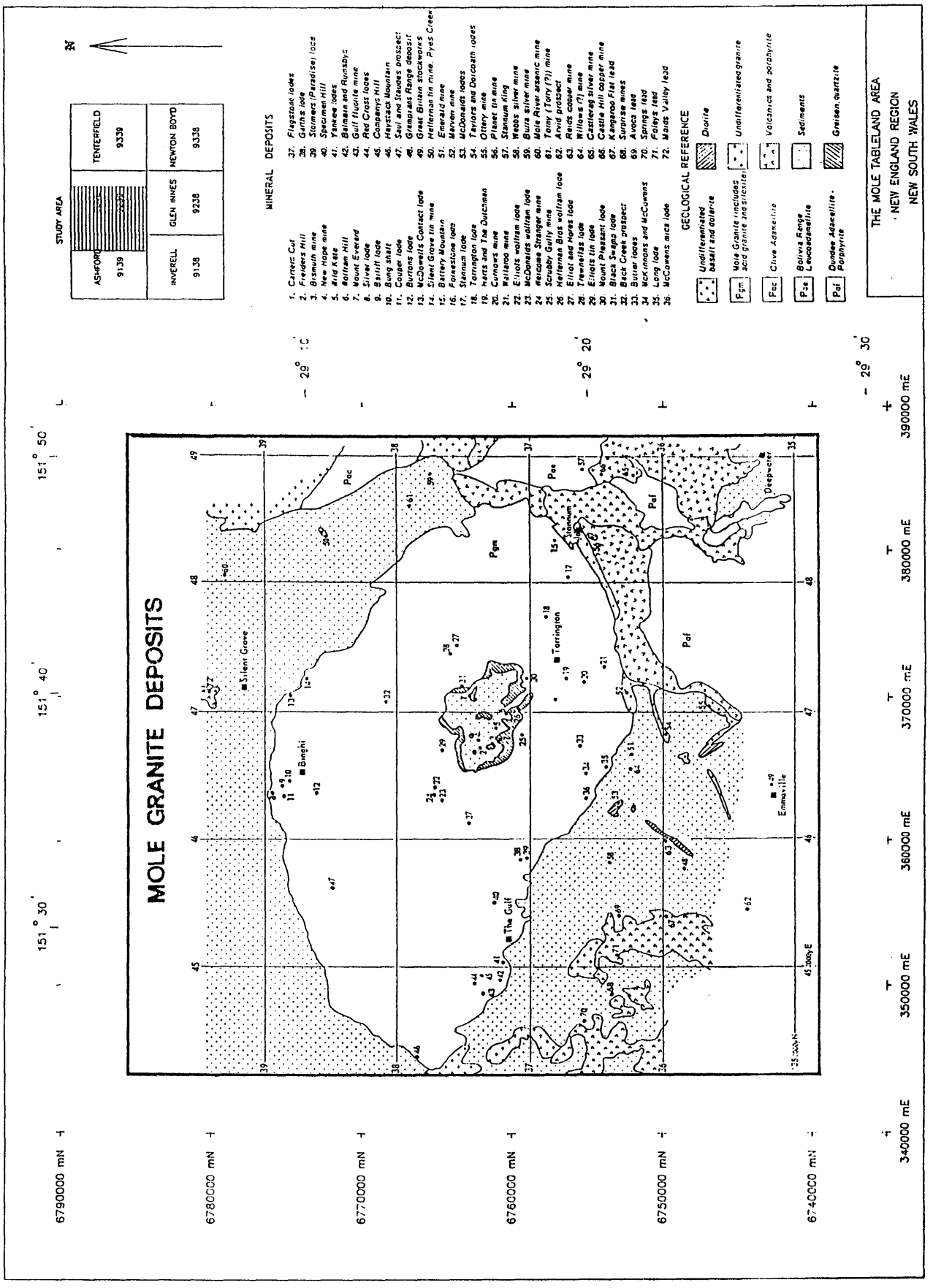

Figure 3.2 Mineral deposits in the Mole Granite and surrounds. (Source: Weber, 1974).

In 1981, Clark used caesium-vapour and proton-precession magnetometers to investigate magnetic anomalies in the Gipsies Range on the northern part of the study area, and has successfully located areas with sulphide mineralizations. Chapman (1983) investigated gravity anomalies of the Ottery Mine Field. Stegmann (1983) examined the Sn-W-Basemetal mineralization on the southern-central margin of the Mole Granite. Baillie (1983) studied geology and mineralization of the Emmaville district. Brodie (1983) studied the geology and mineralization of the Mole River - Silent Grove portion of the northern part of the area. In 1984, Cozens explored the geology and mineralization of the south-west Mole Granite region.

3-2 Previous study on geology and mineralization

Plutonic rocks in the eastern half of the area have been studied by Shaw in 1964 as part of his investigation on the petrology of portion of the New England Batholith, in the Tenterfield region. These include the Clive Adamellite, the Pyes Creek Leuco-Adamellite, and the Bolivia Range Leuco-Adamellite.

Shaw (1964), megascopically, described the Clive Adamellite as a coarse-grained, equigranular rock, with average grainsize of 5 millimetres. The rock is dull-yellow to white in colour, consisting of brecciated amethystine-quartz, white plagioclase, cream-coloured K-feldspar, and plates of biotite.

The Pyes Creek Leuco-Adamellite is a coarse-grained equigranular rocks (average grainsize 5 millimetres). The grainsize becomes finer towards the margin. The rock consists of pinkish K-feldspar and plagioclase, pale-grey quartz and well-disseminated dark biotite. Xenoliths are entirely absent (Shaw, 1964).

The Bolivia Range Leuco-Adamellite has a wide variations in texture, grainsize and mineralogy. It varies from pink medium-grained leuco-granite to porphyritic flesh-coloured adamellite and coarse-grained granite, then to porphyritic adamellite with rapakivi structure. The rapakivi variants show pink-ovoids of K-feldspar mantled by rim of white plagioclase. The average size of the ovoids is 15 millimetres. The groundmass is composed of K-feldspar, plagioclase, and biotite (Shaw, 1964).

In 1982, Godden recognized that the Undifferentiated Granitoids vary in composition, ranging from pink-feldspar leuco-granites and leuco-adamellites to hornblende-bearing adamellites and quartz monzonite. The more acid variants were found to be insignificant. The leuco-granites contain unzoned albitized-plagioclase, quartz, microperthite, granular titanomagnetite, and minor epidotized biotite. Within the same area, leuco-granites with a similar mineralogy are found as rare microxenoliths in hornblende-bearing adamellites (Godden, 1982).

The hornblende-bearing granitoids vary from mafic adamellites and quartz monzonites with seriate hypidiomorphic granular texture to equigranular, medium- to fine-grained leuco-adamellites. The adamellite may contain quartz diorite and rarely granodiorite-xenoliths up to 150 millimetres in diameter. A typical specimen of these granitoids contains quartz, plagioclase, perthitic K-feldspar, amphibole which is accompanied by sphene, magnetite and the exsolved ilmenite, and biotite with inclusions of zircon and apatite. Rare allanite is found only in the leuco-adamellites. Hornblende and biotite are finer in grainsize in the more leucocratic adamellites. They commonly occur as aggregates (Godden, 1982).

Kleeman (1982) described the Mole Granite as a polytextural intrusive, which consists of three principal variants, namely, coarse-grained type, porphyritic and microgranitic.

The coarse-grained type is found away from the margin and in the topographically low areas. The texture is equigranular with alkali-feldspar grains marginally coarser than other minerals. The alkali-feldspar commonly contains mineral inclusions of quartz, plagioclase, and biotite. The biotite is often altered to chlorite and green biotite. Zircon and monazite are common inclusions in the biotite. Plagioclase contains inclusions of quartz, fluorite, topaz, and alkali-feldspar (Baillie, 1983).

The porphyritic variant occurs near the outer margins and at various topographically high points. This rock contains a fine-grained groundmass (average size 0.5 - 1.0 millimetres) and ovoid megacrysts of alkali-feldspar and quartz (3.0 - 20.0 millimetres in diameter). The groundmass is composed of alkali-feldspar, quartz, plagioclase, and dark-reddish-brown biotite, which has been partly altered to chlorite and green-biotite. Zircon, monazite, topaz, muscovite, and fluorite form accessory minerals of the groundmass (Baillie, 1983).

The microgranitic type is found as joint-controlled dykes. It intrudes both of the other two variants. The grainsize of this type is typically 0.3 to 0.5 millimetres, but the grainsize of quartz and alkali-feldspar is found to be up to 5 millimetres in diameter. Topaz is often found as an inclusion in the centre of quartz grains. The red-brown biotite has been altered to chlorite and green-biotite. It occurs as single subhedral flakes interstitial to the quartz and feldspar grains and is more abundant in the microgranite variant than in the other two types (Baillie, 1983).

Baillie (1983) classified the Emmaville Volcanics into four different facies. The rhyolitic ignimbrites are being the major facies. The lesser facies include andesitic lavas, breccias, and epiclastic sediments.

The ignimbrites consist of phenocrysts of quartz and K-feldspar, with minor plagioclase, biotite, and actinolite (Baillie, 1983). The andesitic lavas consist of andesine phenocrysts, minor orthoclase, and chlorite after biotite. The phenocrysts are set in a very fine pilotaxitic groundmass of chlorite, actinolite, feldspar, and quartz (Baillie, 1983). The breccias consist of lithic clasts which are composed predominantly of devitrified glass. The shape of the lithics varies from angular to subrounded with the size ranging from microscopic to 60 millimetres in diameter. Fragments of K-feldspar and quartz also occur in the lithics. The groundmass is composed of devitrified and often recrystallized glass (Baillie, 1983). The epiclastic sediments are composed primarily of angular crystal fragments and subrounded recrystallized lithic clasts. The crystals are mainly quartz and alkali-feldspar with occasional plagioclase and chlorite after biotite, indicative of the rhyolitic source of these sediments (Baillie, 1983).

Baillie (1983) listed the mineralogy of the Tent Hill Porphyrite as follows.

- Quartz is the least abundant of the phenocrysts.

- At the contact with the Mole Granite fine-grained recrystallized quartz is found in the groundmass.

- The most abundant ferromagnesian mineral is biotite.

- Hornblende occurs as an alteration product, metamorphic mineral, or as vein material.

- Augite is rarely altered, and secondary hornblende developed from it.

- The metamorphic hornblende is found only in close proximity to the Mole Granite.

- Calcic amphibole, which may be either actinolite or hornblende, is found as vein material. It occurs in a very intense green colour, and is accompanied by quartz, chlorite, and plagioclase.

- Epidote is ubiquitous throughout the Tent Hill Porphyrite.

- Other minerals found are secondary chlorite, augite, apatite, and sphene.

The Dundee Rhyodacite is composed primarily of phenocrysts of quartz, plagioclase, minor biotite, hornblende, much less clinopyroxene, potassium-feldspar, magnetite, and rarely orthopyroxene. Small gabbroic xenoliths are common. This rock has quartzo-feldspathic groundmass (Baillie, 1983).

3-3 Regional gravity survey

The study area has been covered by a regional gravity survey which was conducted by the Bureau of Mineral Resources (BMR). The result of the survey was published in 1970 as gravity maps of Bouguer anomalies of average rock density of 2.20 g/cc, with contour intervals of 5 milligals at a scale of 1 : 250 000.

The Bouguer anomaly map of the study area and its vicinity is depicted in Figure 3.3 . Negative anomalies ranging from -25 milligals to -50 milligals are prominent in the area. Figure 3.4 shows three profiles of these Bouguer anomalies. The profiles were constructed from known gravity stations on the maps. Over the Mole Granite, deviation of the anomalies from the regional gravity trend is predominantly caused by the negative density contrast between the granite and the surrounding sedimentary rocks. The profiles show that the deviation is within the range of -5 milligals to -15 milligals.

Kleeman (1982) postulated that the shape of the Mole Granite is laminar. The depth of the granite is not unspecified. The granite is relatively thin.

An attempt to test this hypothesis has been made by performing a two-dimensional gravity modelling to investigate the geometry of the Mole Granite. The detail of the gravity modelling is included in Appendix B of this thesis.

The results from the gravity modelling support the hypothesis that the depth of the granite is finite. The geometry shows that the granite is dipping assymetrically towards the north-east. The granite dips are shallower under the sedimentary rocks in the south-west than in the north-east of the Mole Granite. This situation has resulted in a wider area of outcropping contact metamorphic rocks in the south-west than in the north-east, as indicated by Kleeman (1982).

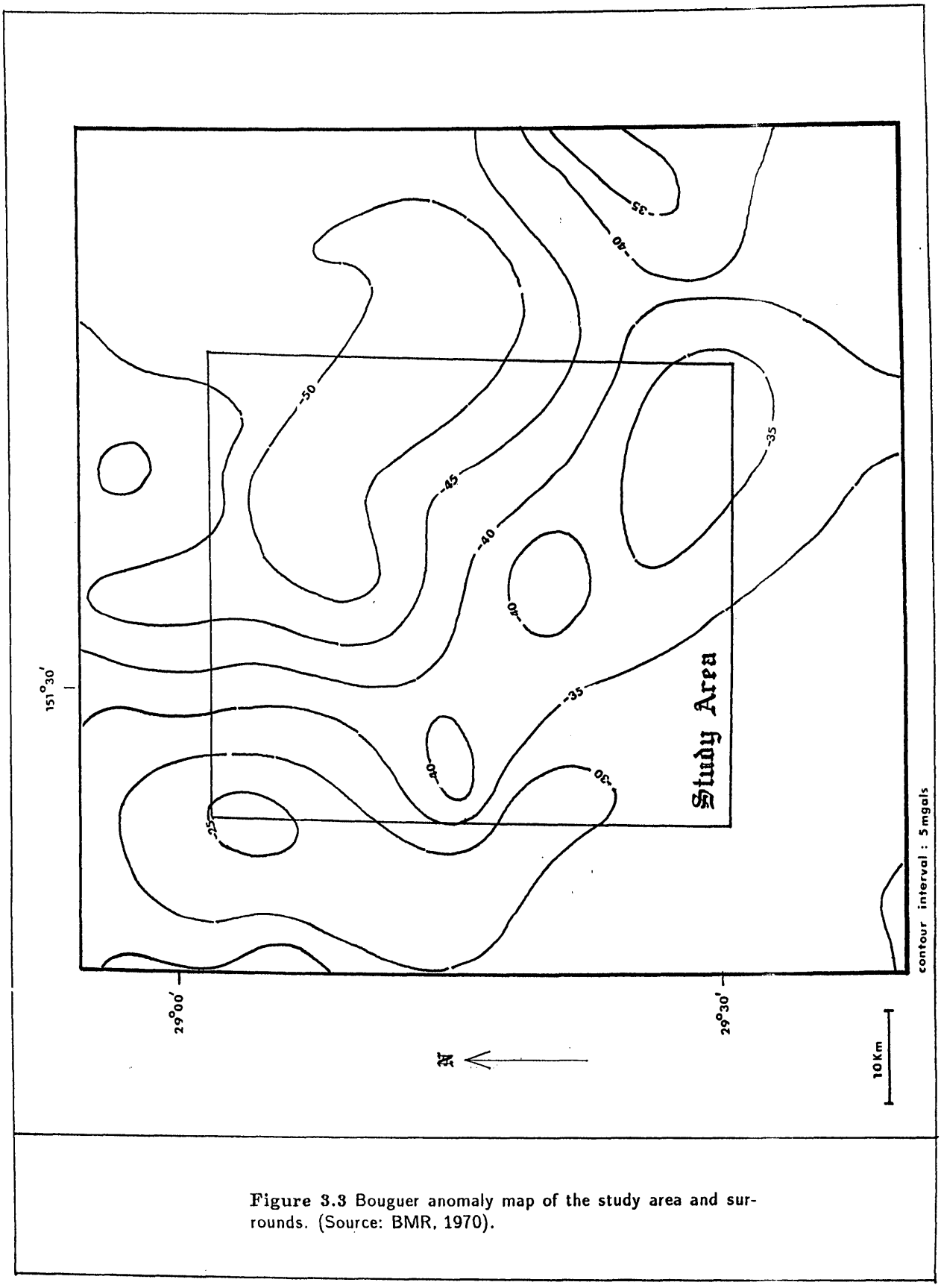

Figure 3.3 Bouguer anomaly map of the study area and surrounds. (Source: BMR, 1970).

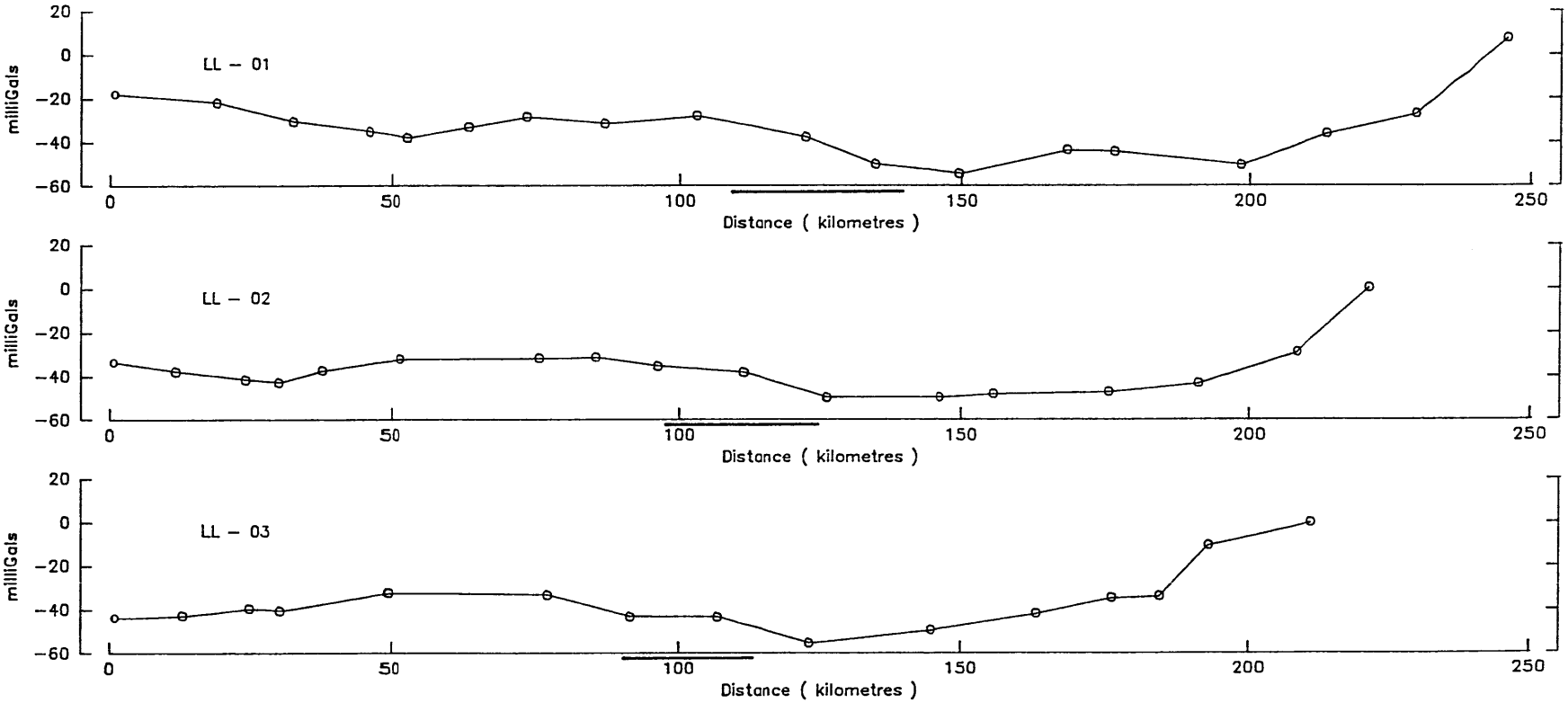

Figure 3.4 Bouguer anomaly profiles over the Mole Granite. Relative position of the outcropped granite is indicated by the heavy lines on the horizontal axes. (Source: BMR, 1970).

3-4 Regional magnetic survey

As part of the regional survey which was conducted by the Department of Mineral Resources of New South Wales, the study area has been recently explored using the aeromagnetic method. The residual of the total aeromagnetic intensity contour map of the area is shown in Figure 3.5 .

The Mole Granite clearly shows featureless aeromagnetic patterns, indicating that the Mole Granite is non-magnetic. This evidence specifies the granite as an "A - type" (Webster, 1984) as suggested by Kleeman (1982).

The high-frequency aeromagnetic response of basalt flows predominates in the area to the mid-south-west of the Mole Granite. The magnetic lineament in the south-east of the Mole Granite coincides with the boundary between the Tent Hill Porphyrite and the Dundee Rhyodacite. This lineament possibly indicates the reconstitution of mineral assemblage resulting from thermal metamorphic effect (Godden, 1976). The high intensities of the magnetic pattern (1850 - 2050 nanoTesla) in the south-east part of the area confirm the magnetite content of the Dundee Rhyodacite as indicated by Baillie (1983).

The Undifferentiated Granite in the north-east shows intense magnetic patterns, with the intensities in the range of 1650 to 1850 nanoTesla. These high-density magnetic patterns signify the mafic content of this granite (Godden, 1982). Furthermore, this unit may be classified as an "I - type" granitoid (Webster, 1984).

Weak or unclear magnetic patterns are obvious in the perimeter of the Mole Granite, indicating that the contact between the granite and the surrounding sediments produced non-magnetic minerals. Weaker aeromagnetic patterns clearly dominate the area to the north-west of the Mole Granite. This area is composed mainly of sedimentary rocks of Carboniferous to Early Permian age (Vickery, 1972).

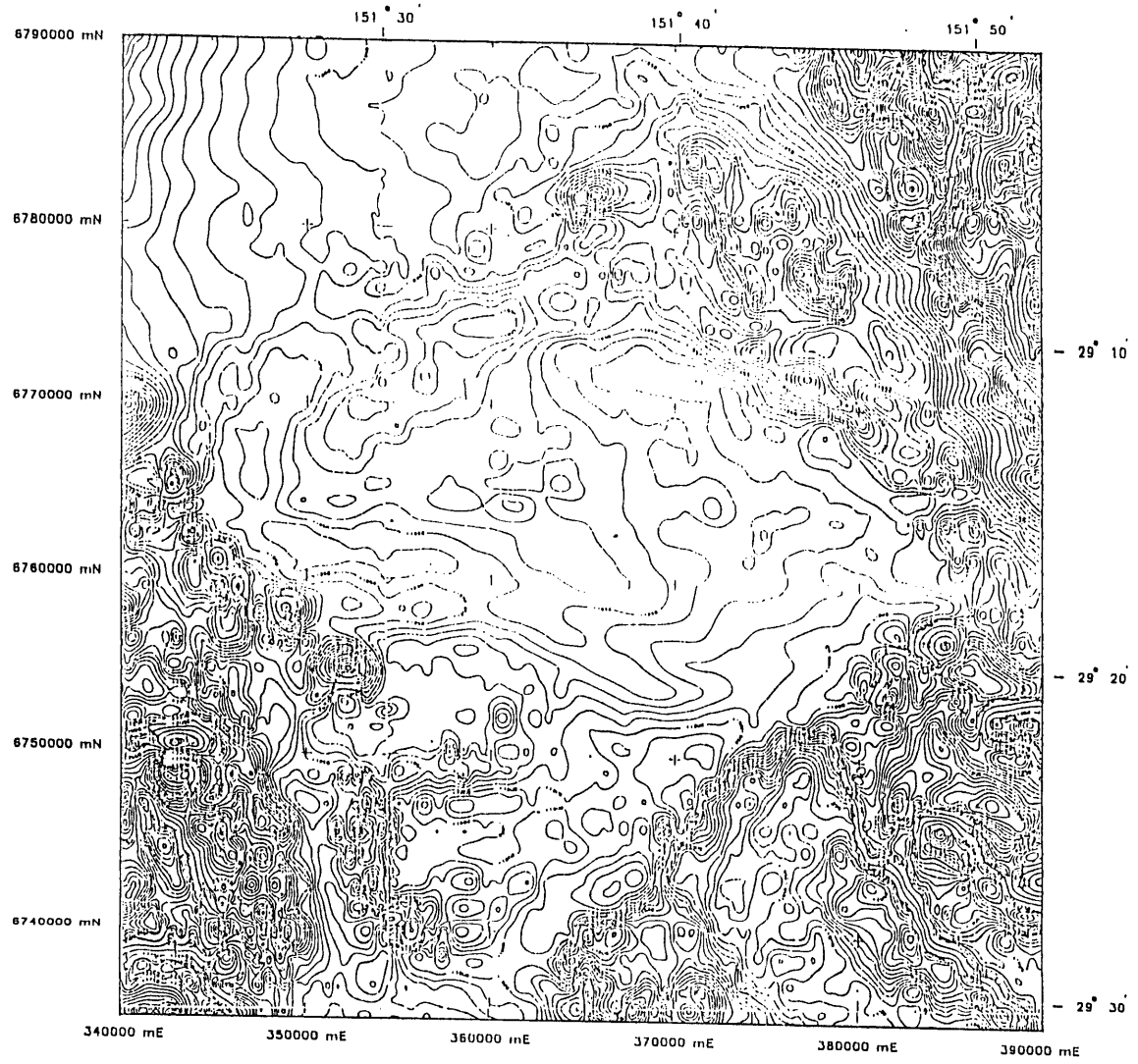

Figure 3.5 Aeromagnetic map of the study area. (Source: Department of Mineral Resources, 1982). Grafton and Inverell Aeromagnetic Sheet.

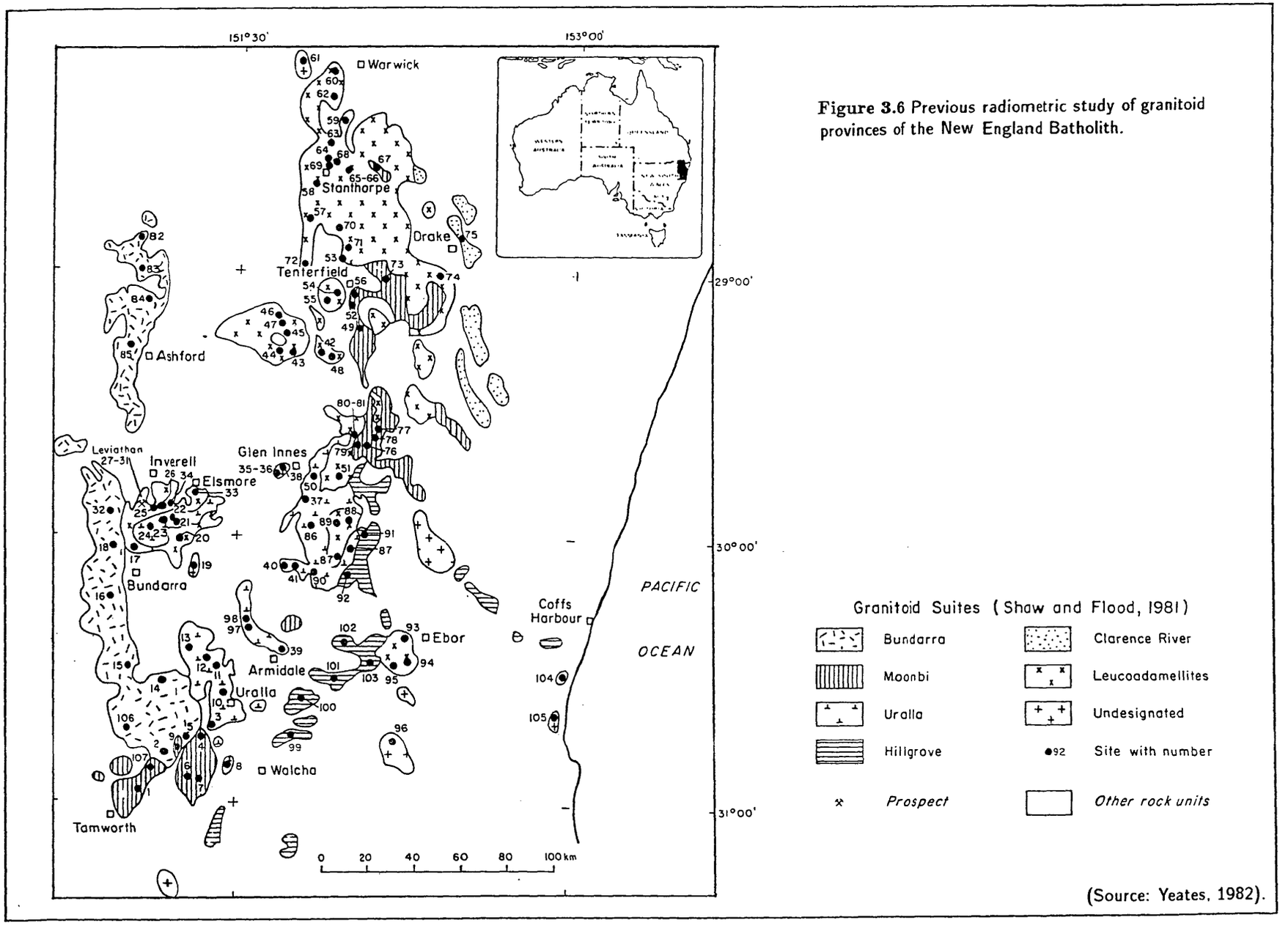

Figure 3.6 Previous radiometric study of granitoid provinces of the New England Batholith.

(Source: Yeates, 1982).

3-5 Previous radiometric survey

In 1982, Yeates determined the radioelement characteristics of tin and tungsten granitoid in the New England Batholith, and other granitoid provinces of south-east Australia (see Figure 3.6).

Measurements of the concentrations of equivalent uranium and equivalent thorium were conducted during a reconnaissance survey using a portable gamma-ray spectrometer. The results of the measurements were evaluated for known mineralized granitoids and compared with values determined from "barren" plutons (Yeates, 1982). Figure 3.7 shows the abundance of the equivalent uranium and equivalent thorium for the six granitoid suites of the New England Batholith. Figure 3.8 illustrates the abundance of equivalent uranium and equivalent thorium for plutons which host cassiterite and wolframite deposits. These plutons have more than 4.00 μg/g equivalent uranium. Among the measurements, five localities on the Mole Granite were visited. These were sites 43, 44, 45, 46, and 47. Results from the measurements at these sites are shown in Table 3-5.1.

The method of Yeates' measurements is, in fact, very dependent on the state of the weathering of the rocks and the relative stability of uranium- and thorium-bearing minerals during the weathering process. A detailed account of the measurements of uranium abundance and rock weathering is given in Enders (1984), and by Guthrie and Kleeman (1986).

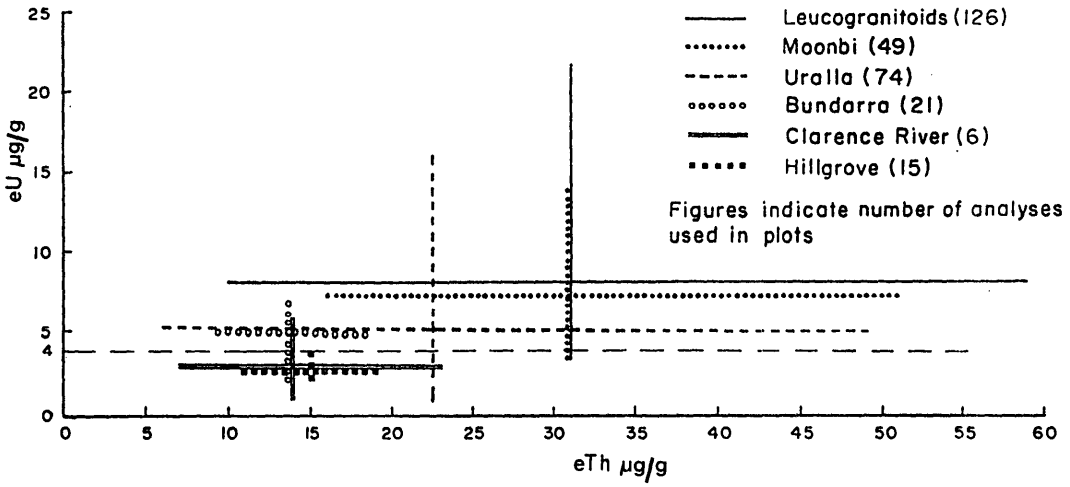

Figure 3.7 The abundance of uranium and thorium in the six granitoid provinces of the New England Batholith. (Source: Yeates, 1982).

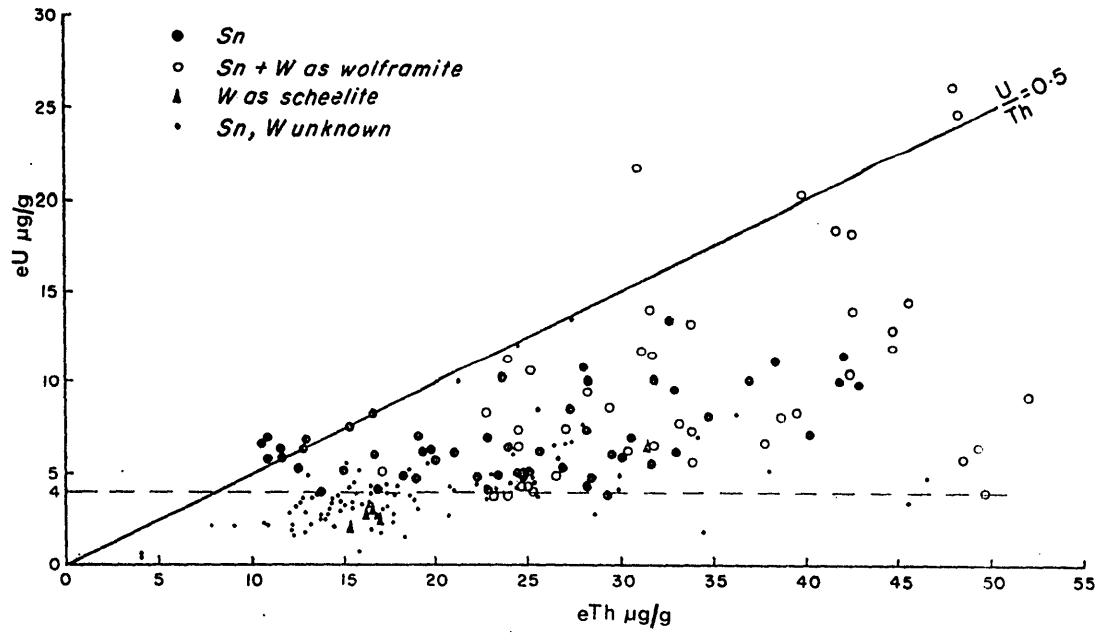

Figure 3.8 Granitoid plutons of the New England Batholith, which host cassiterite and wolframite deposits have more than 4.0 µg/g eU. (Source: Yeates, 1982).

Table 3-5.1

Uranium and thorium content of the Mole Granite
(Source: Yeates, 1982)

Site	Location	eU (µg/g)	eTh (µg/g)
43	29°20' S; 151°45' E	18.4	41.7
		14.1	31.7
44	29°19' S; 151°41' E	4.1	49.7
		9.3	52.1
45	29°15' S; 151°42' E	5.7	33.9
		7.8	33.2
46	29°13' S; 151°42' E	6.5	49.4
		5.8	48.6
47	29°13' S; 151°42' E	7.4	33.9
		6.7	37.9

Chapter 4

THE PRESENT RADIOMETRIC STUDY

4-1 The airborne radiometric survey

The airborne radiometric survey was commissioned by the Department of Mineral Resources of New South Wales in the period of February-March 1982, and flown by the Geometrics International Corporation. The survey has produced 302 flight-lines, which cover approximately 41 470 square kilometres. The study area, which is a portion of the whole survey area, was covered by 96 flight-lines.

The airborne radiometric survey used the Geometrics GR-800 gamma-ray spectrometer, with the NaI(Tl) crystal-detectors assembly of 2048 cubic inches. The Geometrics G-714 data-acquisition system was used for recording the count-numbers of the total radiation, the radiations of ^{40}K, ^{238}U, ^{232}Th as well as cosmic radiation.

Other parameters namely, easting and northing co-ordinates, radar altitude, barometric altitude, fiducial, and time, as well as the aeromagnetic data were recorded on the same magnetic tapes. The aeromagnetic data were not analysed in this study. The aeromagnetic component of the survey was probably the major justification for the data base.

The differential mode of recording was employed for registering of the total radiation counts at the energy window of 0.40 - 3.0 MeV, the ^{40}K radiation counts at 1.37 - 1.57 MeV, the ^{214}Bi radiation counts at 1.66 - 1.87 MeV, and the ^{208}Tl radiation counts at 2.41 - 2.81 MeV.

The airborne radiometric data were sampled at 0.8 second intervals along survey-lines which run east-west and tie-lines running north-south. The nominal flight-line spacing was 1.5 kilometres, and the nominal spacing for tie-lines was 15 minutes of longitude (27.75 kilometres). The nominal survey altitude was 150 metres mean terrain clearance. The flight paths of the survey were recorded on film using the Geocam 35 millimetre continuous-tracking camera. Upward-looking crystals for determining the airborne radon concentration were not used in the survey. The measurements of the combined aircraft and airborne radon background were performed by flying at an altitude 3000.0 feet (914.4 metres) above the ground pre- and post-survey flights daily within the survey area. The energy window of 3.0 - 6.0 MeV were used for monitoring the cosmic-ray background radiation. Test flights were also conducted daily at a predetermined line before and after surveys, to monitor consistency.

4-2 The experimental ground radiometric survey

An experimental ground radiometric survey covering a total distance of 70 kilometres was undertaken at selected lines within the study area. The investigation was conducted in the period of January-March 1984. Figure 4.1 shows the traverses of the survey. The objective of the survey was to closely study the apparent concentration of radioactive elements present on the ground surface, and provide correlation coefficients to the airborne radiometric data.

A Scintrex GAD-6 gamma-ray spectrometer and GSP-4 gamma-ray detector were used in the survey. The GAD-6 spectrometer is a portable, digital, four-channel, spectral-stabilized, gamma-ray analyzer. It allows integral or differential gamma-ray energy analyses with digital counting in four channels simultaneously, registering the count-numbers of the total radiation, the radiations of ^{40}K, ^{214}Bi, and ^{208}Tl. The GSP-4 gamma-ray detector contains a near-cubic NaI(Tl) crystal of the dimensions 2.5"×2.5"×3.5" (360.0 cubic-millimetres) with associated photomultiplier tube, high-voltage power supply, and preamplifier.

The method which was used in the experimental ground radiometric survey investigation was a simulation of the integration of an airborne radiometric survey. While traversing the survey line, the gamma-ray detector was carried by shoulder harness at a height of 800.0 millimetres above the ground. The radiometric data were sampled over periods of 100 seconds, in which time a distance of approximately 100 metres was covered.

Prior to the survey, the calibration of the gamma-ray detector was performed on top of a very large flat surface of a fresh-granite outcrop at the Moonbi Hills road-cutting. The purpose of the calibration was to determine the attenuation factor of the air column between the ground surface and the detector. Figure 4.2 schematically shows the calibration pad on the granite surface.

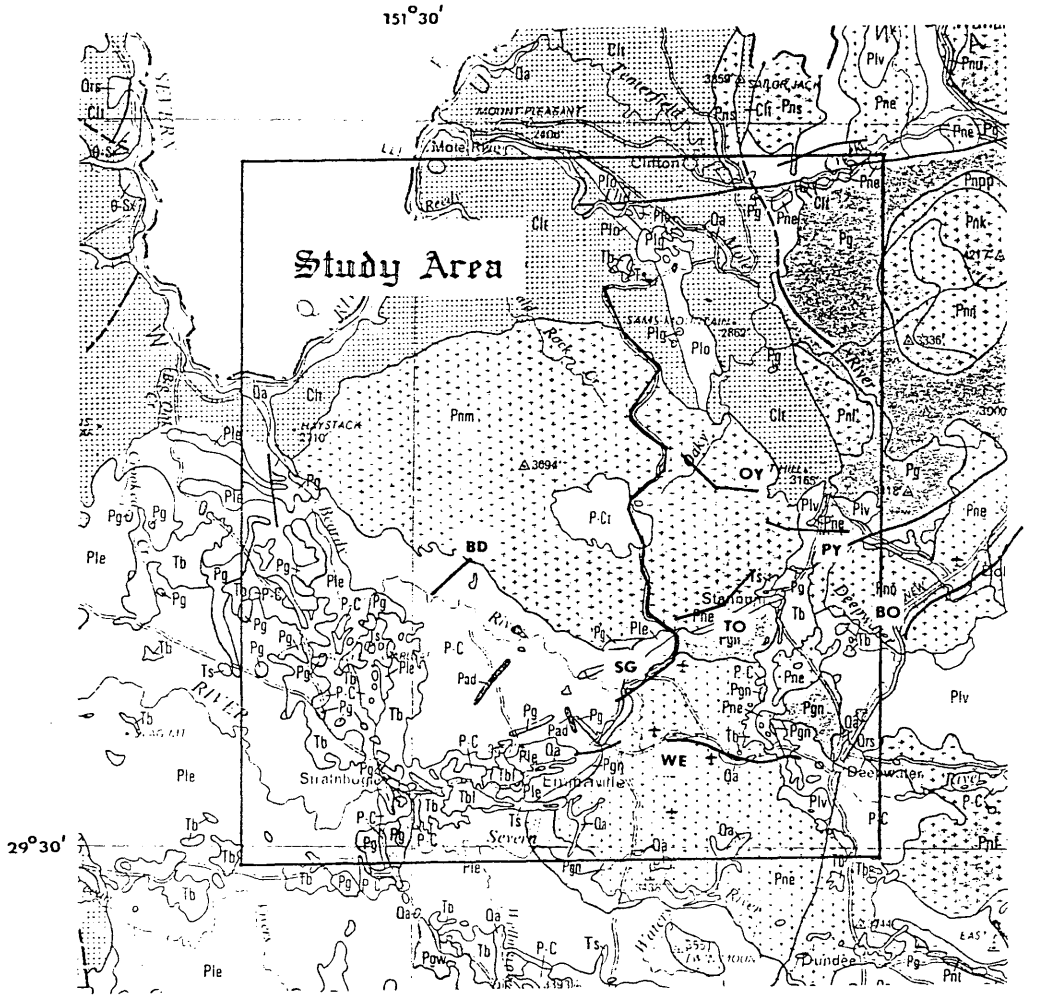

Figure 4.1 Experimental ground radiometric survey traverses.

SG = Silent Grove Road traverse
OY = Oaky Creek traverse
PY = Pyes Creek traverse
TO = Torrington traverse
BD = Beardy River traverse
WE = Wellington Vale traverse
BO = Bolivia Range traverse

(Geology after 1 : 500 000 New England Sheet).

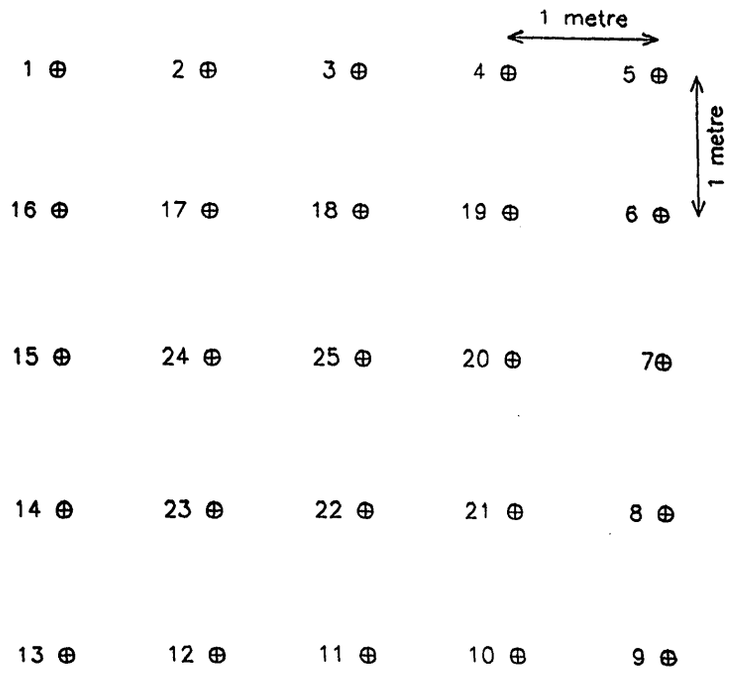

Figure 4.2 Diagrammatic representation of the calibration pad on granite surface.

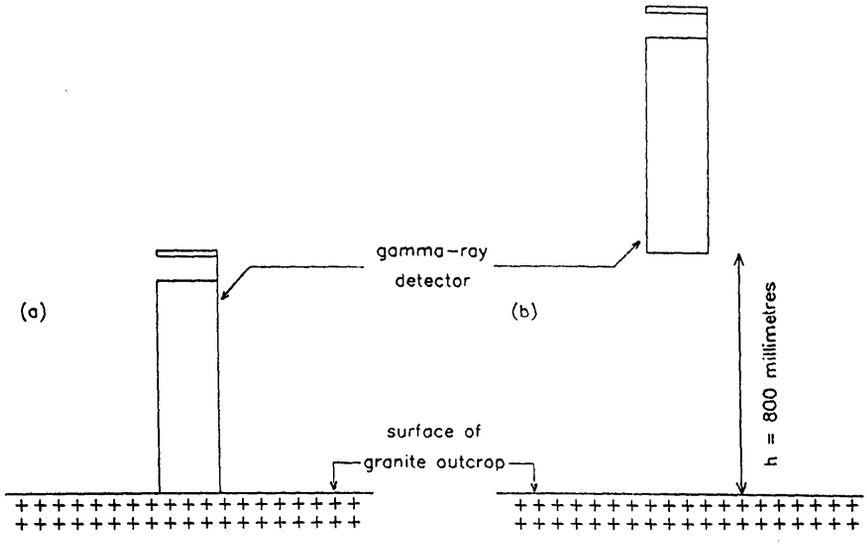

Figure 4.3 Detail of the two types of measurement.
(a) 2π-geometry;
(b) h=800.0 millimetres.

A 4 by 4 metres flat surface of the granite outcrop was gridded into 5 by 5 equally-spaced measurement-points. Two types of measurements were conducted; these were of 2π-geometry in contact with the outcrop and measurement at a height of 800.0 millimetres above the surface. Figure 4.3 details the position of the detector in the two types of measurement, 2π-geometry (a) and h = 800.0 millimetres (b).

In the 2π-geometry method, every grid point was measured once, except the innermost point which was measured twice, at the beginning and the end of the 2π-geometry method. In the measurement at the height of 800.0 millimetres, grid points 1 to 16 were occupied once, grid points 17 to 24 were measured twice, and the innermost point (grid point number 25) was measured three times. Figure 4.4 illustrates occupation of the grid points. Numbers on the grid points indicate the sequence of the measurements taken on the particular grid. Tables 6-3.1 and 6-3.2 show the results of the measurements.

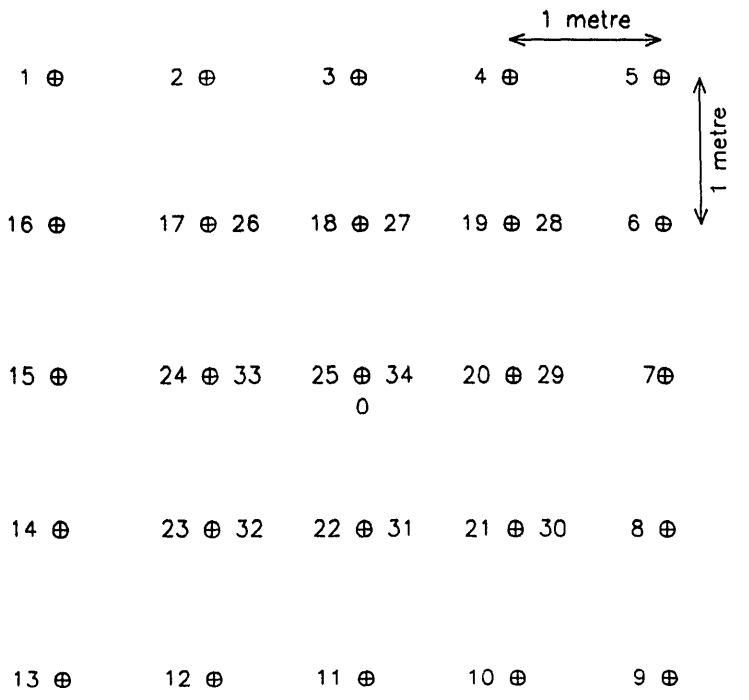

Figure 4.4 Sequence of measurements of the grid points in the calibration of the GSP-4 gamma-ray detector.

The attenuation factors which were obtained from the experiment were used in processing the experimental ground radiometric survey data.

The intensities of the cosmic and instrumental background radiation were determined by taking measurements on the Dumaresq dam, west of Armidale, and on a two-hectare dam on the Mc Inness property in Torrington. Figure 4.5 shows the situation when background measurement was performed.

The consistency of data-reading was periodically examined using the uranium- and thorium-standard specimens supplied with the instrument. It was also checked by taking a set of readings on a check-pad on a relatively flat granite outcrop at the beginning and the end of each day's work. Figure 4.6 shows one of the check pads used in the Silent Grove Road radiometric investigation,the Wallaroo check-pad, which is located near the southern contact between the Mole Granite and the sediments.

Figure 4.5 Measurement of background radiation on a two-hectare dam in Torrington, NSW.

Figure 4.6 Wallaroo check-pad near the southern contact between the Mole Granite and sediments.

4-3 Laboratory gamma-ray spectrometric analysis

The main objective of the laboratory analysis was to determine the concentration of radioactive elements K, U, and Th in rock samples collected from several locations within the study area. Four standard rock samples were used as references. These were the international standard rocks GSP-1, G-2, AGV-1, and BCR-1. The background radiation data were obtained from dunite rock sample which contains negligible thorium, uranium, and potassium.

The analysis was performed employing an ORTEC-6240 multichannel gamma-ray spectrum analyzer with a BICRON 75mm × 75mm NaI(Tl) detector. The full gamma-ray spectrum of the rock sample was recorded over 1024 channels.

The counting chamber consists of a two-litre cylindrical free space which is shielded by 3000 kilograms of lead, giving an effective thickness of 110 millimetres. Figure 4.7 is the cross-section diagram of the counting chamber.

The typical display of the gamma-ray spectrum which emerges on the CRT-screen of the analyzer is shown in Figure 4.8 .

The digital data obtained from the analyzer can be transferred into the University's DEC-2060 computer on completion of the counting period. The data may then be processed and plotted on a digital-incremental plotter. Figure 4.9 shows the computer-processed gamma-ray spectrum of the rock sample taken from the Wallaroo check-pad.

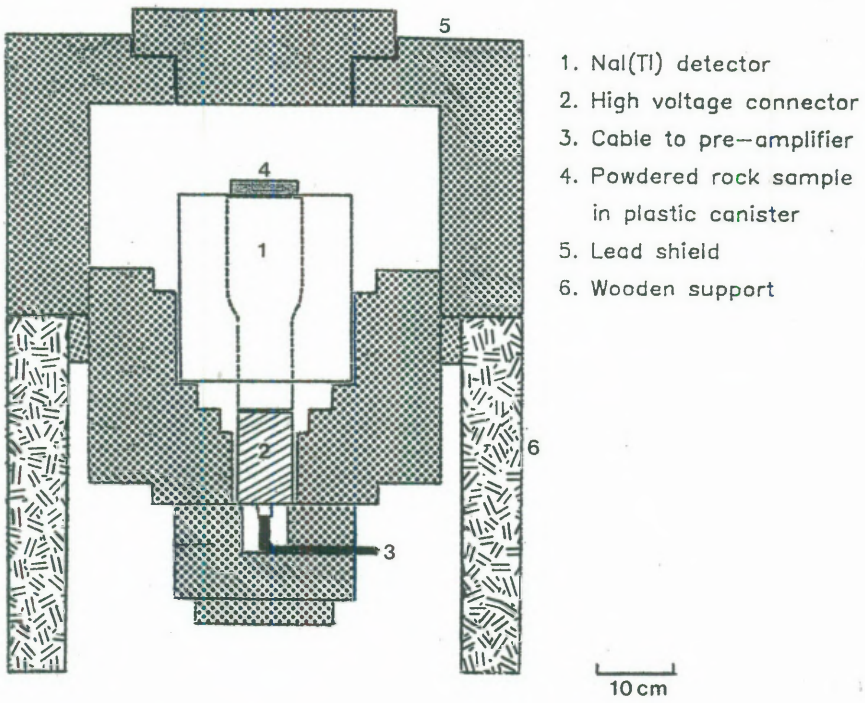

Figure 4.7 Cross-section diagram of the counting chamber.

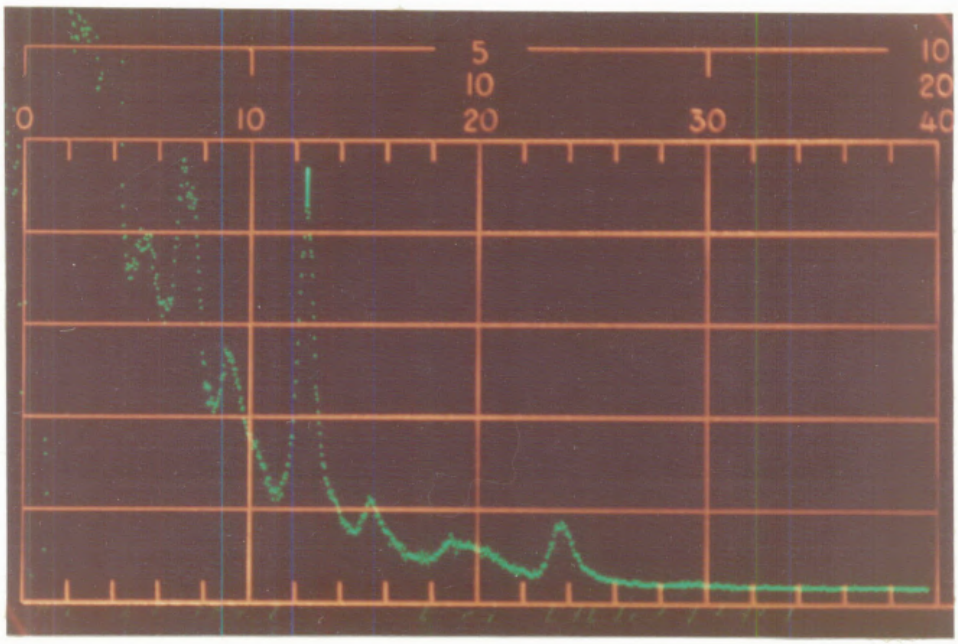

Figure 4.8 Gamma-ray spectrum display of the ORTEC-6240 spectrometer.

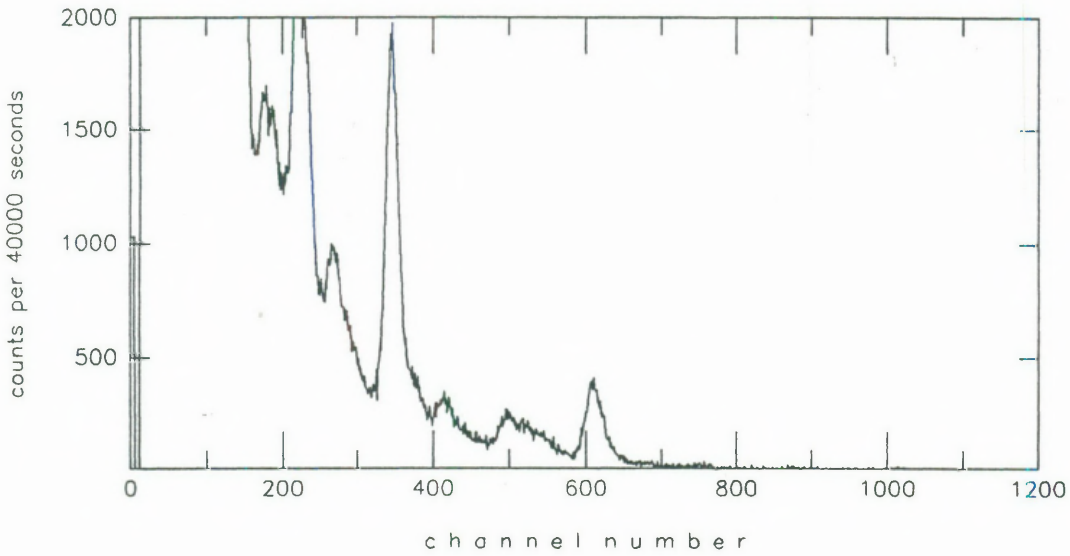

Figure 4.9 Gamma-ray spectrum of a rock specimen collected from the Wallaroo check-pad.

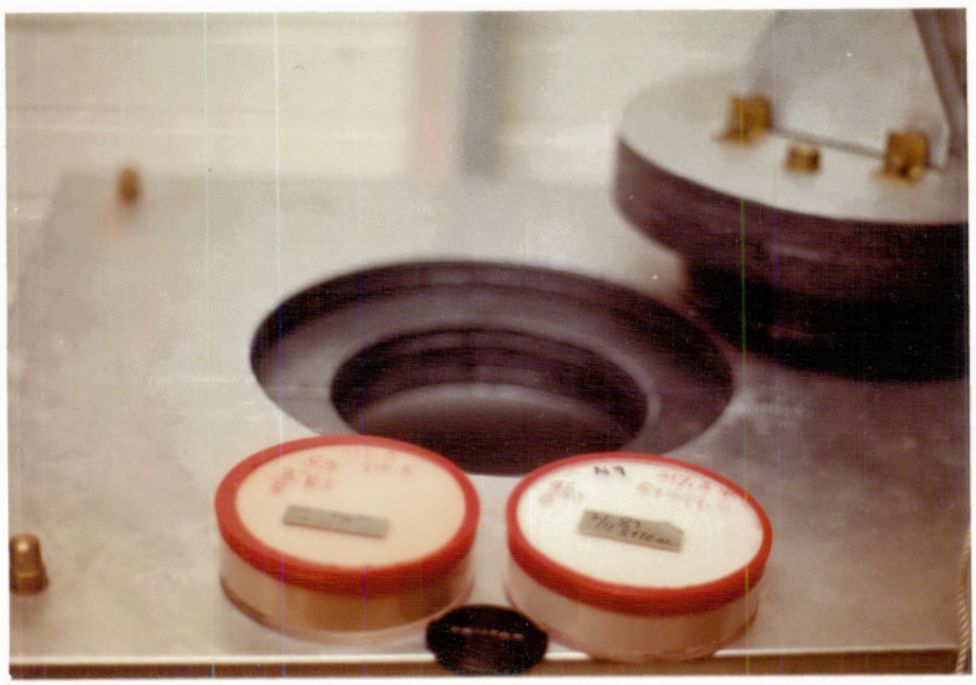

Figure 4.10 Powdered rock specimens contained in plastic canisters ready for analysis.

The preparation of rock samples for the analysis involves:

- collecting a 2 kilograms rock in the field;
- using a 5 kilograms hammer, to break the rock into approximately 200 grams rock-chips;
- crushing the rock-chips on the Chipmunk jaw crusher to produce rock-fragments of the size of approximately 10 to 20 millimetres;
- further crushing employing a 0.75 kilowatt excentric crusher to produce rock-powder.

Prior to the analysis, the rock-powder is transferred into a plastic canister, and kept for at least 21 days before analysis commences in order to achieve equilibrium. Approximately 300 to 600 grams rock-powder, depending on the rock type, is required to fill the plastic canister and maintain constant sample geometry, since the homogenity of the powder in the canister influences the result of the analysis. Figure 4.10 shows the photograph of the plastic canisters which were used in the analysis.

Polynomial curve-fitting was employed to fit the observed spectrum data against the analytical curve. The purpose of the curve-fitting was to locate the analytical energy-spectrum peaks of ^{40}K, ^{214}Bi, and ^{208}Tl of every rock sample. Table 6-4.1 shows the results obtained from the laboratory gamma-ray spectrometric analysis.